จุฬาลงกรณ์มหาวิทยาลัย

ทุนวิจัย

กองทุนรัชดาภิเษกสมโภช

รายงานวิจัย

สมบัติของผิวผลึกเซอร์โคเนียและการดูดซับโมเลกุลก๊าซชนิดต่างๆ

โดย

วิทยา เรืองพรวิสุทธิ์

กันยายน ๒๕๕๘

CHULALONGKORN UNIVERSITY

RESEARCH FUND

RATCHADAPHISEKSOMPHOT ENDOWMENT FUND

RESEARCH REPORT

SURFACES PROPERTIES OF ZIRCONIA AND ITS ADSORPTION OF GASES

BY

VITHAYA RUANGPORNVISUTI

SEPTEMBER 2015

ACKNOWLEDGMENTS

The authors gratefully acknowledge the financial support from the Ratchadaphiseksomphot Endowment Fund, Office of Research Affairs, Chulalongkorn University, Contact Number R 005 2557.

บทคัดย่อ

การดูดซับก๊าซ CO และ NH_3 บนผิวคิวบิคของ ZrO_2 (110) ได้รับการสอบสวนโดยวิธีเดนซิตีฟังก์ชันนัล ชนิดขอบเขตคาบแบบสองมิติ พบว่าลำดับพลังงานดูดซับของก๊าซดังกล่าว บนผิวชนิดคิวบิคของ ZrO_2 (110) เป็นดังนี้: NH_3 > CO พลังงานดูดซับของก๊าซ NH_3 บนผิวชนิดคิวบิคของ ZrO_2 (110) มีค่าเท่ากับ –27.62 และ –25.51 kcal/mol ได้รับจากการคำนวณโดยวิธี PBE0 และ B3LYP ตามลำดับ พลังงานดูดซับของก๊าซ CO บนผิวชนิดคิวบิคของ ZrO_2 (110) มีค่าเท่ากับ –11.39 และ –9.81 kcal/mol ได้รับจากกการคำนวณโดยวิธี PBE0 ด้วยการจำลองแบบแข็งเกร็งและแบบยืดหยุ่น ตามลำดับ

การหาโครงสร้างวัสดุนาโนเซอร์โคเนีย (ZrO_2–NP) โดยใช้ $(ZrO_2)_{12}$ ซึ่งเป็นคลัสเตอร์ที่เสถียรมีสมมาตรสูงเป็นตัวแทน และการหาโครงสร้างการดูดซับวัสดุนาโนเซอร์โคเนีย (ZrO_2–NP) กับก๊าซชนิดสองอะตอม (H_2, N_2, O_2, CO and NO), ชนิดสามอะตอม (CO_2, N_2O, NO_2, H_2O, SO_2 and H_2S) และชนิดหลายอะตอม (C_2H_2, C_2H_4, CH_4 and NH_3) โดยวิธีเดนซิตีฟังก์ชันนัล พลังงานการดูดซับของสารประกอบดังกล่าวบน ZrO_2–NP คำนวณโดยวิธี B3LYP และ M06–2X การหาโครงสร้างวัสดุนาโนเซอร์โคเนียที่ถูกโด๊ปด้วยอะตอมเดี่ยวของโลหะแทรนซิชัน M (M–ZrO_2–NP) ได้แก่การโด๊ปด้วยธาตุ Sc, Ti, V, Cr, Mn, Fe, Co, Ni, Cu และ Zn รวมถึงการหาค่าพลังงานแถบของสารประกอบดังกล่าว และการหาโครงสร้างการดูกซับก๊าซไฮโดรเจนบน M–ZrO_2–NP โดยวิธี B3LYP การแนะนำอย่างเป็นไปได้ว่า Cu–ZrO_2–NP เป็นวัสดุที่ใช้ในการตรวจวัดก๊าซไฮโดรเจนได้

ABSTRACT

The adsorption of CO and NH_3 gases on the cubic ZrO_2 (110) surface was investigated by two–dimensionally periodic slab model DFT method. The relative adsorption energies of these gases on the cubic ZrO_2 (110) surface is in order: NH_3 > CO. The adsorption energies of NH_3 on the cubic ZrO_2 (110) surface are –27.62 and –25.51 kcal/mol, obtained using the PBE0 and B3LYP methods, respectively. The CO adsorption on the cubic ZrO_2 (110) surface –11.39 and –9.81 kcal/mol, obtained using the PBE0 with rigid and flexible models, respectively.

The geometry optimizations of zirconia nanoparticle (ZrO_2–NP), represented by the high symmetric $(ZrO_2)_{12}$ cluster and its adsorption configurations with diatomic (H_2, N_2, O_2, CO and NO), triatomic (CO_2, N_2O, NO_2, H_2O, SO_2 and H_2S) and polyatomic (C_2H_2, C_2H_4, CH_4 and NH_3) gases were carried out using density functional theory method. Adsorption energies of the relevant gases on the ZrO_2NP were obtained by the B3LYP and M06–2X methods. The geometry optimizations of ZrO_2–NP doped by single metal (M) atoms such as Sc, Ti, V, Cr, Mn, Fe, Co, Ni, Cu and Zn were obtained using the DFT/B3LYP method. Energy gaps of all the relevant compounds obtained B3LYP calculations are reported. The adsorption structures of hydrogen gas adsorbed on the M–ZrO_2–NP and their adsorption energies were obtained using the B3LYP/GEN computation. The Cu–doped ZrO_2–NP has probably been suggested to be a material for use in detecting hydrogen gas.

TABLE OF CONTENTS

LIST OF ILLUSTRATIONS

Figure **Page**

LIST OF TABLES

LIST OF ABBREVIATIONS

B1WC	The Becke one–parameter hybrid functional combined with the Wu–Cohen functional.
B3LYP	The Becke three–parameter hybrid functional combined with the Lee–Yang–Parr correlation functional
c–ZrO_2	Cubic ZrO_2
C<u>O</u>	CO gas points its O toward target atom
DFT	Density functional theory method
ECP	Effective core potential
GEN	General basis set, keyword allows a user–specified basis set to be used
LanL2DZ	Los Alamos National Laboratory 2–Double–Z
M	Metal
M06–2X	Minnesota (Truhlar and Zhao) hybrid functional with 54% HF exchange
m–ZrO_2	Monoclinic ZrO_2
M–ZrO_2–NP	Zirconium dioxide nanoparticle doped with M metal atom
O<u>C</u>	CO gas points its C toward target atom
O_{1C}	One–fold coordinated oxygen atom
O_{2C}	Two–fold coordinated oxygen atom
PBE0	The Perdew-Burke-Ernzerh of hybrid functional
t–ZrO_2	Tetragonal ZrO_2
TMs	Transition metals
WC1LYP	The Wu–Cohen one–parameter with the Lee–Yang–Parr correlation functional
ZrO_2–NP	Zirconium dioxide nanoparticle
Zr_{4C}	Four–fold coordinated zirconium atom

LIST OF SYMBOLS

C_1	C_1 point group of symmetry
C_{2V}	C_{2V} point group of symmetry
ΔE_{ads} (kcal/mol)	Adsorption energy
E_{FPU} (kcal/mol)	Formation energy per unit
E_{gap} (eV)	HOMO–LUMO energy gap
E_{HOMO} (eV)	Highest Occupied Molecular Orbital Energy
E_{LUMO} (eV)	Lowest Unoccupied Molecular Orbital Energy
E_{OF} (kcal/mol)	Overall formation energy
ΔE_{rel} (kcal/mol)	Relative energy
E_{total} (au)	Total energy

CHAPTER I

INTRODUCTION

1.1 The CO and NH_3 adsorption on the ZrO_2 (110) surface

Zirconium oxide demonstrates three structural polymorphs, namely monoclinic (m–ZrO_2), tetragonal (t–ZrO_2) and cubic phases (c–ZrO_2). The tetragonal phase (P42/nmc) and cubic phase (Fm3m) are unstable at room temperature but at atmospheric pressure above 1170 ^oC and 2370 ^oC, respectively [1]. The m–ZrO_2 is stable at below 1000 ^oC. Nevertheless, ZrO_2 is able to form a range of subtoichiometric oxides ZrO_{2-X} which presents defective ZrO_2 and able to adsorb many elementary gases such as CO_2 [2], CO [2], N_2O [3], NO_X [4–7], H_2O [8] and H_2 [9]. Photocatalytic decomposition of water over ZrO_2 powder was first examined by Sayama and Arakawa [10]. ZrO_2 was utilized as support material which can dramatically promote the activity of the supported metal catalysts [11–13], due to its acidity and basicity surface called bifunctional property [14–16]. It has the oxidizing and reducing properties [17] and the high thermal stability which is good quality for catalyst and support [18]. The mechanism of CO_2 reaction with methanol over the ZrO_2 to synthesize dimethyl carbonate (DMC) was studied [19]. The combined CO_2 reforming and partial oxidation of *n*-heptane on various noble metal zirconia catalysts was studied [20]. The adsorption of elementary gases on the ZrO_2 should affect decomposition of hydrocarbon compounds such as naphthalene [21] and tar [22–25]. To understand properties insights of the effect of gas components of hydrocarbon compounds decomposition, the adsorption of elementary gases on the ZrO_2 surface maybe theoretically investigated. The adsorptions of selected gases, CO and NH_3 on the c–ZrO_2 with (110) plane have been studied.

1.2 Gases adsorption on the zirconia nanoparticle

Zirconium dioxide (ZrO_2) is a stable material and to be chemically and thermally inert. ZrO_2 has been found as an important material widely used as heterogeneous

catalysts [26–29], ceramics [30] and gas sensors [31]. Different types of ZrO_2 were widely used as catalytic promoters [32–34]. Different crystal structures of ZrO_2 molecules were found that their band gaps are within the range of 3.25 to 6.1 eV [35–46]. Adsorption of hydrogen on the tetragonal ZrO_2 (101) surface was theoretically studied for [47]. The molecular structures and energetics of the $(ZrO_2)_n$ (n = 1–4) Clusters and their anions were theoretically studied [48]. The structures and electronic structures of $(ZrO_2)_n$ (n = 1–6) clusters and their hydrogen adsorptions were investigated using density functional theory and found that H_2 can easily adsorbed on the top Zr atoms of the clusters [49] and H_2 adsorbed on the ZrO_2 was investigated by DFT method [50]. Nevertheless, the structures of $(ZrO_2)_n$ (n = 1–12) clusters were optimized using B3LYP/GEN of which basis sets for zirconium and oxygen atoms are LanL2Dz and 6-31G(d), respectively, see Chapter II. All the structures of $(ZrO_2)_n$ (n = 1–12) clusters and their energetics are shown in Figure A1 and Table A1 in Appendix, respectively. Only one $(ZrO_2)_{12}$ clusters conformer of was selected as the zirconia nanoparticles (ZrO_2–NPs).

As small gases adsorptions on the ZrO_2–NPs have been useful information for their adsorption abilities and reactions, the $(ZrO_2)_{12}$ cluster of which the structure is a high symmetry molecule has been selected as ZrO_2–NPs representative. Due to the selected $(ZrO_2)_{12}$ cluster has C_{2v} point group of which the dipole lies along the rotation axis, it contains two types of Zr center and its molecule is composed of fourfold coordinated Zr atom (Zr_{4C}) and twofold coordinated O atom (O_{2C}), see Figure 1.1. The surface of the selected $(ZrO_2)_{12}$ cluster can also be categorized into two characteristics as (1) planar and (2) concave Zr centers as shown in Figure 1.1.

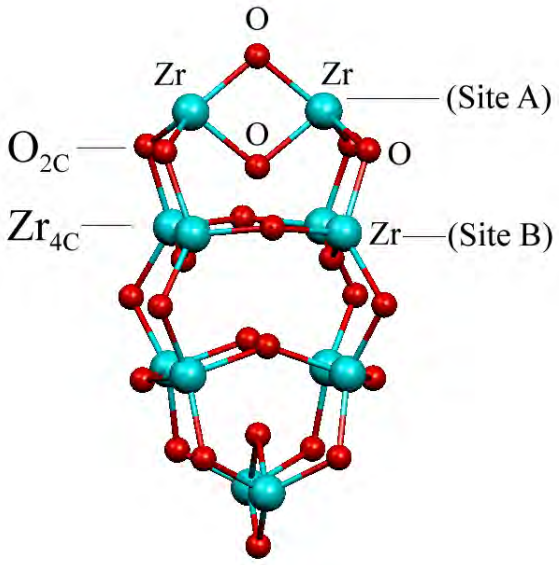

Figure 1.1 The $(ZrO_2)_{12}$ cluster with C_{2v} point group structure as representative for the zirconia nanoparticle (ZrO_2–NP). The planar and concave Zr centers as two types of adsorption sites (A and B) are shown.

1.3 Enhancement of metal–doped zirconia nanoparticle

Electronic and magnetic properties of Fe–doped ZrO_2 was studied by experimental and theoretical methods [51] and magnetic properties of transition metals (TMs) doped ZrO_2 [52–56] were investigated. High Curie temperature (Tc) in TMs doped ZrO_2 were theoretically predicted [57,58]. As the ceramic properties, the state of Ti dopants at the unreduced and reduced (111) surfaces of cubic zirconia was investigated. It was found that Ti is a thermodynamically favorable process and prefers to remain at the ceramic surface rather than migrate to the bulk [59]. As the catalytic properties, the Cu–doped ZrO_2 was found to be catalyst for CO_2 hydrogenation to methanol [60].

1.4 Objectives

In order to provide fundamentally information for zirconia (ZrO_2) which is potential and thermal stable material as catalysts for useful reactions using small gases as reactants and/or gas sensors, adsorptions of small gases on different surfaces of ZrO_2 have therefore been studied. Materials of zirconia doped with metal atoms have also been studied for their adsorption abilities. Adsorptions of gases on surfaces of the ZrO_2 (110), the zirconia nanoparticle (ZrO_2–NP) and their metals doping materials have been theoretically investigated as follows.

(1) The adsorption of CO and NH_3 adsorption on the ZrO_2 (110) surface has been studied using periodic DFT method.

(2) The structure of the $(ZrO_2)_{12}$ cluster which has point group of C_{2v} symmetry and its adsorption configurations with gases H_2, N_2, O_2, CO, NO, CO_2, N_2O, NO_2, H_2O, SO_2 H_2S, CH_4, C_2H_4, C_2H_2 and NH_3 have been studied using DFT methods. Electronic properties of all adsorption structures have been investigated. Adsorption energies of these gases adsorption on the ZrO_2–NP have been determined.

(3) As metal–doped ZrO_2–NPs have been expected to be high ability for gases adsorption, in this work, metal (M)–doped ZrO_2–NPs where M is a metal atom of Sc, Ti, V, Cr, Mn, Fe, Co, Ni, Cu and Zn, have therefore been studied for their structures, electronic properties and adsorption ability on weak interaction gas molecule such as hydrogen gas.

CHAPTER II

EXPERIMENTS

2.1 Computational method for the ZrO_2(110) system

2.1.1 Adsorption of gases on the ZrO_2(110) surface

All DFT calculations of two–dimensionally periodic slab model have been carried out using the CRYSTAL06 computational code [61], based on the expansion of the crystalline orbitals as a linear combination of a basis set consisting of atom centered Gaussian orbitals. The Kohn–Sham orbitals as Gaussian–type–orbital basis sets of double zeta quality as an 32111dfG which is a fitting effective core potential (ECP) and an 8–411G contraction scheme have been respectively employed for the zirconium [62] and oxygen [63] atoms on the ZrO_2 (110) surface.

Basis set for carbon, oxygen, hydrogen and nitrogen atoms of adsorbates employed in this calculations are a 631d1G [64], an 8411dG [65], 31p1G [66] and a 631dG [66], respectively except for carbon atom of methane adsorbed on the ZrO_2 (110) surface, the 6311d11G [65] being used. The hybrid functionals, B3LYP including Becke's three–parameter exchange [66] and Lee–Yang–Parr correlation [67], PBE0 [68–70] have been employed. As the optimized bulk lattice parameters for the cubic ZrO_2 were examined under different DFT methods, B1WC [71], B3LYP, PBE0 and WC1LYP [67,72] hybrid functionals with varying of shrink CRYSTAL06 parameter, the bulk lattice parameters obtained by the B3LYP method with shrink (4,4) (a = 5.1299 Å) and PBE0 with shrink (2,2) (a = 5.1127 Å) are closed to the experimental parameter of 5.1291 Å, respectively [73]. The cubic ZrO_2 as crystal class of cubic hexakisoctahedral has Fm3m space group. The computed lattice parameters of the ZrO_2 with Fm3m space group using different DFT methods are shown in Table 2.1. It shows that the PBE0 and B3LYP methods result the space parameter "a" closed to experimental result of the X–ray crystallographic [73] as most and second most reliable, respectively.

The Monkhorst–Pack scheme for 8×8×8 k–point mesh in the Brillouin zone was applied for cubic ZrO_2 crystal. In geometry optimizations of two–dimensionally periodic slab, the lattice constants were fixed at these values while the positions of all zirconium and oxygen atoms were allowed to relax.

The cubic ZrO_2 (110) was modeled as [3×3] slab with four layers. Two models, rigid and flexible models are defined as all surface atoms being fixed and atoms in two outer layers being allowed to move, respectively. The tolerances for geometry optimization convergence have been set to the default values [61] and the coulomb–exchange screening tolerances were set to (7, 7, 7, 7, 14). All slab calculations have been performed with a Monkhorst–Pack [74] k–point grid with shrinking factors (2,2) for BPE method and (4,4) for B3LYP method. There are two binding sites for the cubic ZrO_2 (110) surface: three–fold–coordinate oxygen atom (O_{3C}) and six–fold–coordinate zirconium atom (Zr_{6C}) as shown in Figure 2.1.

Table 2.1 Computed lattice parameters of the ZrO_2, with space group Fm3m using different DFT methods.

Parameter	DFT [a]	DFT [b]	DFT [c]	DFT [d]	Exp [e]	DFT [f]
a, *b*, *c* [g]	5.0974	5.1614	5.1127	5.1434	5.1291	5.22
α, *β*, *γ* [h]	90.00	90.00	90.00	90.00	90.00	90
Cell volume [i]	132.4	137.5	133.6	136.1	134.9	–

[a] B1WC method.

[b] B3LYP method.

[c] PBE0 method.

[d] WC1LYP method.

[e] Ref. [73].

[f] Ref. [75].

[g] The lattice constants are in Å.

[h] The lattice constants are in degree.

[i] The lattice constants are in $Å^3$.

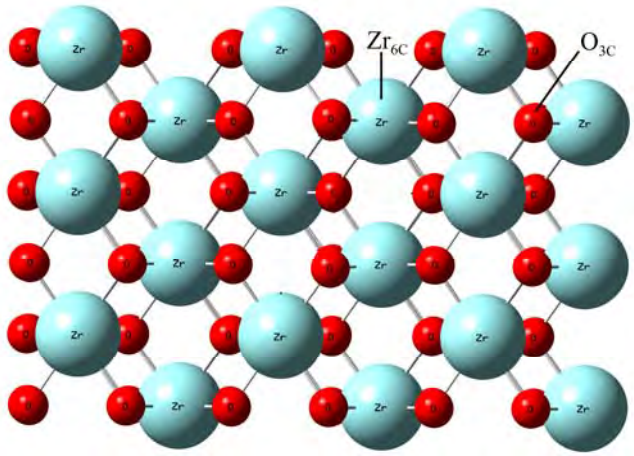

Figure 2.1 The cubic ZrO_2 (110) surface slabs of the full optimized crystal using PBE0 method shows its top view. Atoms at the surface show their three–fold–coordinate O atom (O_{3C}) and six–fold–coordinate Zr atom (Zr_{6C})**.**

2.2 Computational method for the ZrO_2–NP system

2.2.1 Adsorption of gases on the ZrO_2–NP

Full optimizations of structures of the ZrO_2–NP represented by the $(ZrO_2)_{12}$ cluster and adsorption configurations of H_2, N_2, O_2, CO, NO, CO_2, N_2O, NO_2, H_2O, SO_2 H_2S, CH_4, C_2H_4, C_2H_2 or NH_3 gas on the ZrO_2–NP were carried out using density functional theory (DFT) method. Optimizations for single molecule and twelve molecules adsorptions of NO and NO_2, their total electronic states of doublet (spin multiplicity=2) state were applied. The calculations have been performed with hybrid density functional B3LYP, the Becke's three–parameter exchange functional [76] with the Lee–Yang–Parr correlation functional [77], and hybrid density functional M06–2X [78], using two effective core potential (ECP) basis sets, the Los Alamos LanL2DZ split–valence basis set [79–81] for Zr atom and 6–31G(d) [82] for all other atoms. Calculations were performed with the GAUSSIAN 09 program [83].

The adsorption energies (ΔE_{ads}) for single molecules of relevant gases namely H_2, N_2, O_2, CO, NO, CO_2, N_2O, NO_2, H_2O, H_2S, SO_2, C_2H_2, C_2H_4, CH_4 or NH_3 adsorbed on the ZrO_2–NP have been obtained using Equation (2.1).

$$\Delta E_{ads}\,(\text{Gas}) = E(\text{Gas/ZrO}_2\text{–NP}) - [E(\text{ZrO}_2\text{–NP}) + E(\text{Gas})] \quad (2.1)$$

where E(Gas/ZrO_2–NP) is the total energy of gas molecule adsorbed on the ZrO_2–NP, E(Gas) and E(ZrO_2–NP) are the total energies of isolated adsobate Gas and free ZrO_2–NP, respectively.

2.2.2 Selection for ZrO_2–NP representative

The $(ZrO_2)_{12}$ cluster which represents the ZrO_2–NP was selected from the B3LYP/GEN–optimized structures of four conformations, $(ZrO_2)_{12}$_a, $(ZrO_2)_{12}$_b, $(ZrO_2)_{12}$_c and $(ZrO_2)_{12}$_d, as shown in Figure 2.2. All four conformations are composed of four–fold coordinated Zr atom (Zr_{4C}) and two–fold coordinated O atom (O_{2C}) except one atom of oxygen on $(ZrO_2)_{12}$_c which is one–fold coordinated O atom (O_{1C}). The relative energies of four conformers are shown in Table A1, in Appendix. The $(ZrO_2)_{12}$_a cluster which is a molecule with C_{2v} point–group symmetry and moderately stable (ΔE_{rel} = 13.55 kcal/mol as compared with the most stable conformer, $(ZrO_2)_{12}$_b cluster) was selected. The B3LYP/GEN−optimized structures of $(ZrO_2)_n$ where n= 1 to 12, are shown in Figure A1, in Appendix.

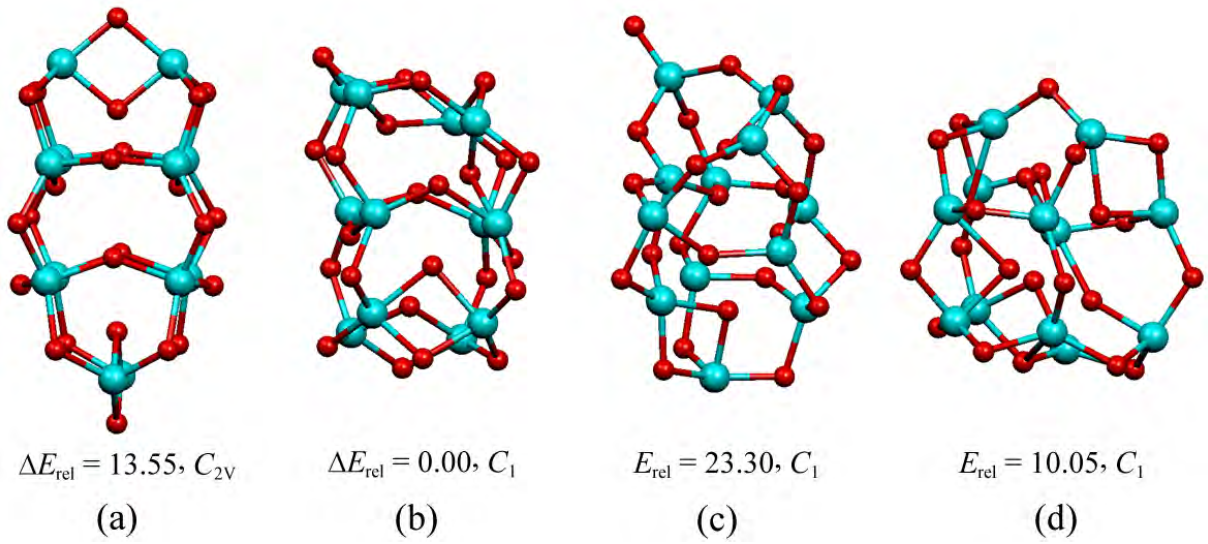

Figure 2.2 The B3LYP/GEN–optimized structures of four conformations (a) $(ZrO_2)_{12}$_a, (b) $(ZrO_2)_{12}$_b, (c) $(ZrO_2)_{12}$_c and $(ZrO_2)_{12}$_d. Their relative energies (in kcal/mol) and point groups of symmetry are shown at the bottom. The cyan and red balls are Zr and O atoms, respectively.

2.2.3 Definition of metal atom doping on the zirconia nanoparticle

The structures of zirconia nanoparticle (ZrO_2–NP) doped by single atom of metal M which denoted by M–ZrO_2–NP are defined and compared with non–doped zirconia nanoparticle. Doping definition is defined as a single metal atom M substitutes the Zr atom labeled by Zr1. The hydrogen gas adsorption on the ZrO_2–NP is defined that M dopant atom is the adsorption site.

2.2.4 Test for the accurate DFT method via energy gap

Energy gaps of the ZrO_2–NP obtained from DFT/B3LYP and DFT/M06–2X methods were compared with the experiment. The DFT method which results the energy gap of the ZrO_2–NP being close to the experiment will be used in all calculations.

CHAPTER III

RESULTS AND DISCUSSION

3.1 Adsorption of CO and NH_3 on the ZrO_2(110) surface

The cubic ZrO_2 (110) surface slab of the full optimized crystal using PBE0 method shows their three–fold–coordinate O atom (O_{3C}) and six–fold–coordinate Zr atom (Zr_{6C}) as shown in Figure 2.1. The adsorption geometries of NH_3 and CO on the ZrO_2 (110) surface are shown in Figures 3.1 and 3.2, respectively. Figure 3.1 shows similar structures of NH_3 adsorbed on the ZrO_2 (110) surface computed by PBE0 and B3LYP methods. The adsorption energies for NH_3 and CO on the ZrO_2 (110) surface computed at various models of the PBE0 and B3LYP methods are listed in Table 3.1.

The relative adsorption energies of NH_3 and CO on the cubic Zr_2 (110) surface is in order: NH_3 > CO. The adsorption energies of NH_3 on the cubic ZrO_2 (110) surface are –27.62 and –25.51 kcal/mol, obtained using the PBE0 and B3LYP methods, respectively. The CO adsorption on the cubic ZrO_2 (110) surface –11.39 and –9.81 kcal/mol, obtained using the PBE0 with rigid and flexible models, respectively.

Table 3.1 Adsorption energies of CO and NH_3 on the ZrO_2 (110) surface, computed at various models of the PBE0 and B3LYP methods.

Adsorbate	ΔE_{ads} [a,b]		ΔE_{ads} [a,c]	
	Rigid model	Flexible model	Rigid model	Flexible model
CO	–11.39	–9.81	– [d]	– [d]
NH_3	– [d]	–27.62	– [d]	–25.51

[a] In kcal/mol.

[b] Using PBE0 method.

[c] Using B3LYP method.

[d] No result is obtained.

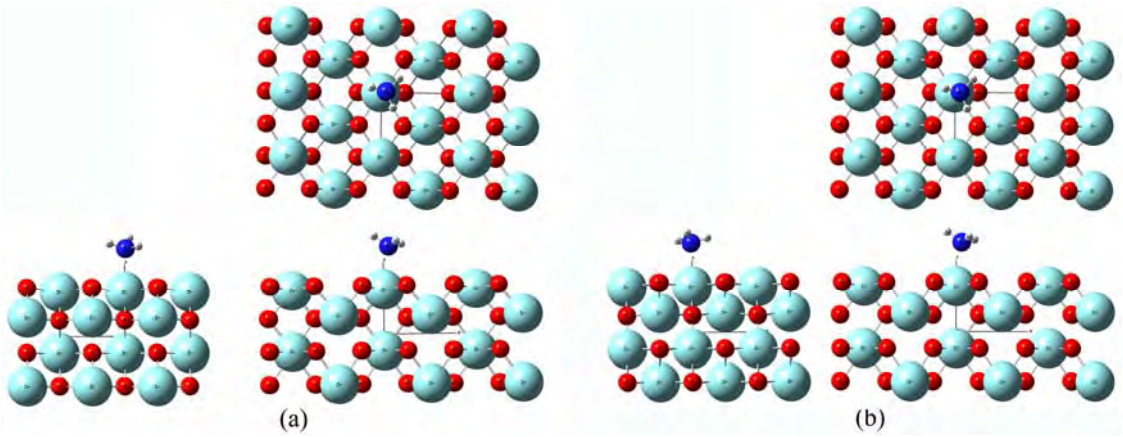

Figure 3.1 The adsorption structure for NH_3 on the ZrO_2 (110) surface computed by (a) periodic PBE0 method with three layers flexible model using CRYSTAL06–parameter shrink (2,2) and (b) B3LYP method with three layers flexible model using CRYSTAL06–parameter shrink (4,4). Left, right and top images are side, front and top views, respectively.

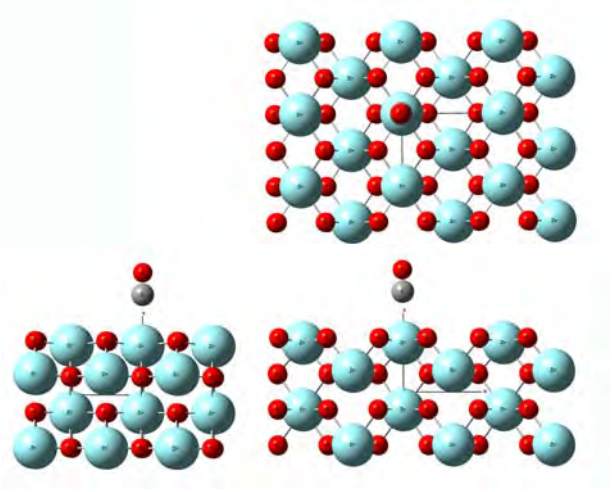

Figure 3.2 The adsorption structure for CO on the ZrO_2 (110) surface computed by periodic PBE0 method with three layers flexible model using CRYSTAL06–parameter shrink (2,2). Left, right and top images are side, front and top views, respectively.

3.2 Structure of the C_{2v} symmetry $(ZrO_2)_{12}$ cluster as representative of the ZrO_2–NP

The B3LYP/GEN–optimized structures of $(ZrO_2)_n$ (n = 1–12) clusters and their energetics are shown in Figure A1 and Table A1 in Appendix, respectively. If low–energy conformers of $(ZrO_2)_n$ (n = 1–12) clusters which differences of their relative energies less than 15 kcal/mol were selected, restricted numbers of conformers are taken into account. These conformers are able to be as follows: $(ZrO_2)_2$_a, $(ZrO_2)_2$_b, $(ZrO_2)_2$_c, $(ZrO_2)_3$_a, $(ZrO_2)_3$_b, $(ZrO_2)_3$_c, [$(ZrO_2)_4$_a], $(ZrO_2)_5$_a, $(ZrO_2)_5$_f, $(ZrO_2)_6$_a, $(ZrO_2)_6$_b, $(ZrO_2)_7$_b, $(ZrO_2)_7$_c, $(ZrO_2)_8$_a, $(ZrO_2)_8$_b, $(ZrO_2)_8$_c, $(ZrO_2)_8$_d, $(ZrO_2)_8$_e, $(ZrO_2)_8$_a, $(ZrO_2)_9$_c, $(ZrO_2)_{10}$_b, $(ZrO_2)_{10}$_c, $(ZrO_2)_{11}$_b, $(ZrO_2)_{11}$_c, $(ZrO_2)_{12}$_a, $(ZrO_2)_{12}$_b and $(ZrO_2)_{12}$_d.

The structure optimizations for the ZrO_2–NP, represented by the stable $(ZrO_2)_{12}$ cluster with C_{2v} point–group symmetry were carried out using DFT/B3LYP and DFT/M06–2X methods. The B3LYP/GEN– and M06–2X/GEN–optimized structures for the ZrO_2–NP are shown in Figure 3.3. The geometrical parameters obtained by the B3LYP/GEN and M06–2X/GEN methods are somewhat similar as shown in Table 3.2.

3.3 Adsorptions of single molecules of gases on the ZrO_2–NP

The B3LYP/GEN–optimized structures of adsorption configurations of single molecule of diatomic (H_2, N_2, O_2, CO and NO), triatomic (CO_2, N_2O, NO_2, H_2O, SO_2 and H_2S) and polyatomic (C_2H_2, C_2H_4, CH_4 and NH_3) gases on the ZrO_2–NP are shown in Figures 3.4, 3.5 and 3.6, respectively. They show that there are two adsorption configurations for CO (O<u>C</u>/ZrO_2–NP and C<u>O</u>/ZrO_2–NP), NO (O<u>N</u>/ZrO_2–NP and N<u>O</u>/ZrO_2–NP) and N_2O (O<u>N_2</u>/ZrO_2–NP and N_2<u>O</u>/ZrO_2–NP) adsorbed on two adsorption sites (A and B) of the ZrO_2–NP. The underlined atomic symbol is defined as atom in adsorbate gas which points toward the Zr adsorption site on the ZrO_2–NP. Thus, O<u>C</u>/ZrO_2–NP means that the adsorption complex which CO gas points its C atom toward Zr atom on the ZrO_2–NP. Relative energies either obtained from the B3LYP/GEN or M06–2X/GEN methods result that stabilities of these three pairs of adsorption configurations shown in Table 3.3 are in orders: O<u>C</u>/ZrO_2–NP(A) > O<u>C</u>/ZrO_2–NP(B) >

C<u>O</u>/ZrO_2–NP(A) > C<u>O</u>/ZrO_2–NP(B), O<u>N</u>/ZrO_2–NP(A) > N<u>O</u>/ZrO_2–NP(A) > O<u>N</u>/ZrO_2–NP(B) > N<u>O</u>/ZrO_2–NP(B) and N_2<u>O</u>/ZrO2–NP(A) > O<u>N_2</u>/ZrO2–NP(A) > N_2<u>O</u>/ZrO2–NP(B) > O<u>N_2</u>/ZrO2–NP(B).

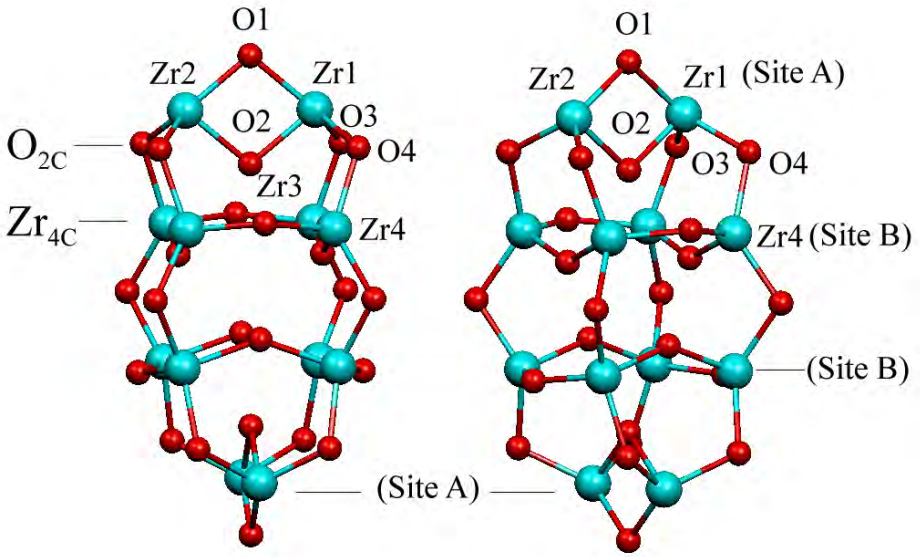

Figure 3.3 The structure of zirconia nanoparticle (ZrO_2–NP), represented as the most stable $(ZrO_2)_{12}$ cluster. The two different views are shown. Two types of adsorption sites (A and B) are over the Zr1 and Zr4 atoms.

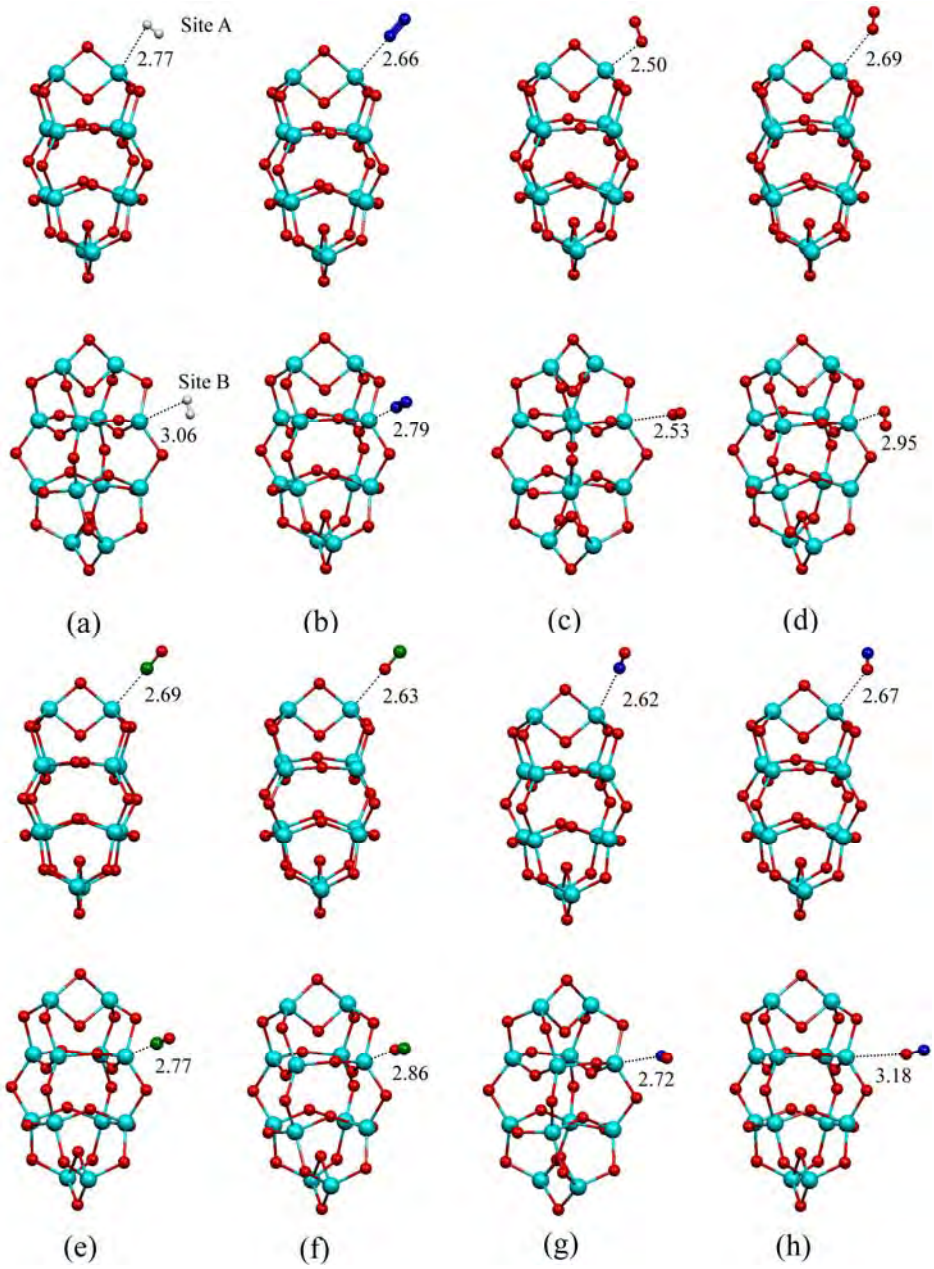

Figure 3.4 Adsorption structures of (a) H_2, (b) N_2, (c) O_2 and (d) Triplet–state O_2, (e) C<u>O</u> (its O toward Zr atom), (f) O<u>C</u> (its C toward Zr atom), (g) N<u>O</u> (its O toward Zr atom) and (h) O<u>N</u> (its N toward Zr atom) on adsorption sites A (top image) and B (bottom image) of ZrO_2–NP. Bond distances are in Å.

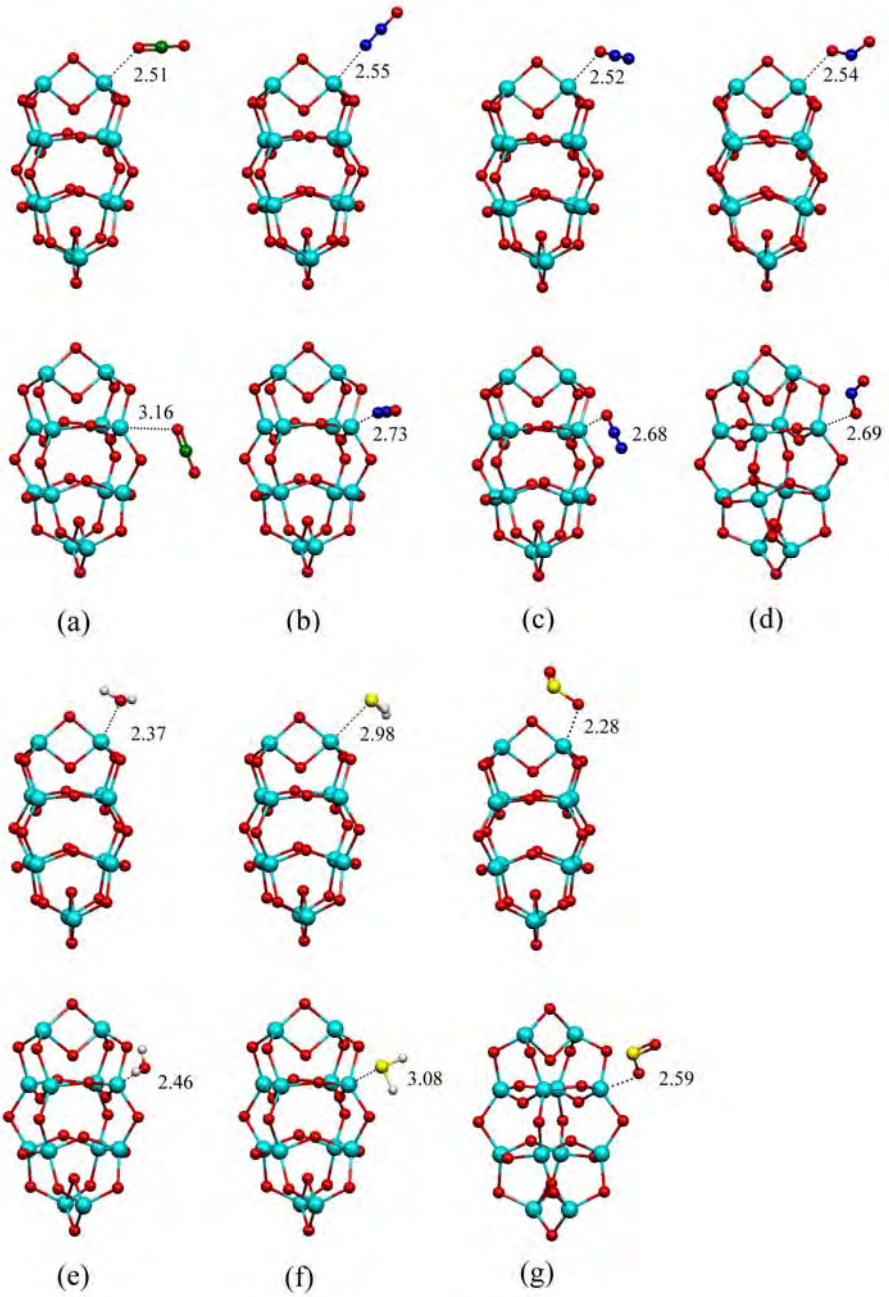

Figure 3.5 Adsorption structures of (a) CO_2, (b) $\underline{N}_2O$ (its N toward Zr atom), (c) $N_2\underline{O}$ (its O toward Zr atom), (d) NO_2, (e) H_2O, (f) H_2S and (g) SO_2 on adsorption sites A (top image) and B (bottom image) of ZrO_2–NP. Bond distances are in Å.

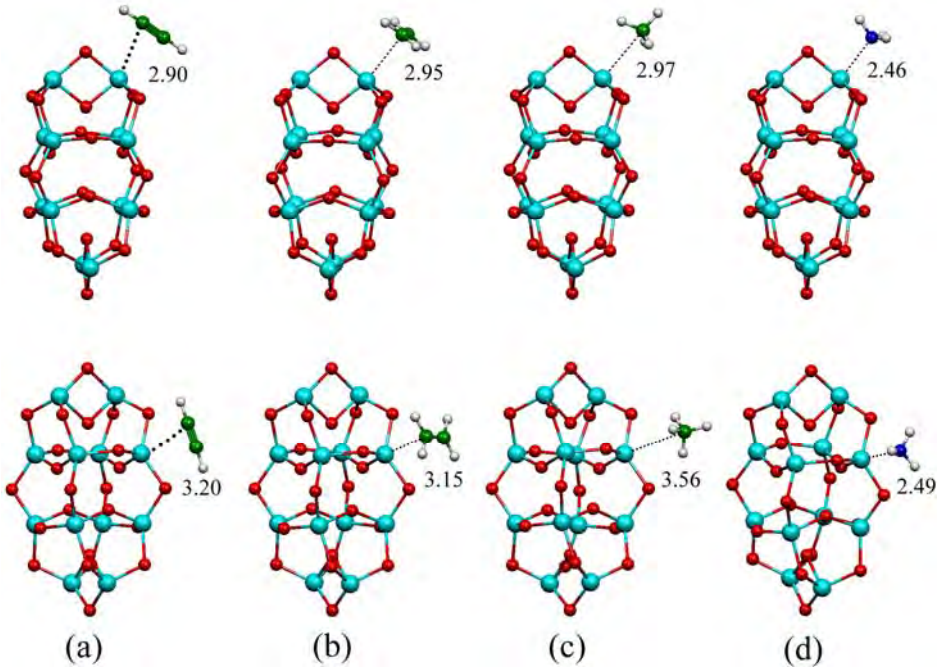

Figure 3.6. Adsorption structures of (a) C_2H_2, (b) C_2H_4, (c) CH_4 and (d) NH_3 on adsorption sites A (top image) and B (bottom image) of ZrO_2–NP. Bond distances which are in Å.

Structural rearrangements of all the adsorption configurations are indicated by geometrical parameters for gas adsorption toward Zr atom which is the adsorption–site on the ZrO_2–NP, computed at the B3LYP/GEN and M06–2X/GEN levels of theory are tabulated in Table A2, in Appendix.

Table 3.2 The selected geometrical parameters for zirconia nanoparticle (ZrO_2–NP), computed at two different DFT methods.

Parameters [a]	B3LYP/GEN [b]	M06–2X/GEN [b]
Bond lengths: [c]		
Zr1–O1, Zr2–O1	2.03	2.02
Zr1–O2, Zr2–O2	2.02	2.04
Zr1–O3, Zr1–O4	1.98	1.96
Zr3–O3	2.03	2.03
Bond angle: [d]		
O1–Zr1–O2	79.30	79.76
O1–Zr1–O3	126.67	127.16
Dihedral angle: [d]		
O1–Zr1–O3–Zr3	–100.56	–98.26
Zr2–O1–Zr1–O3	85.47	84.61
Zr2–O2–Zr1–O3	–126.82	–127.45

[a] Labeling of atoms is shown in Figure 3.3.

[b] GEN defined that the LanL2DZ basis set is used for the Zr atom and 6–31G(d) for O atom.

[c] In Å.

[d] In degrees.

Table 3.3 Relative energies of adsorption configurations for CO, NO or N_2O on the ZrO_2–NP, computed at the B3LYP/GEN and M06–2X/GEN levels of theory.

Gas adsorption	ΔE_{rel} [a]			
	B3LYP/GEN		M06–2X/GEN	
	Site A[b]	Site B[b]	Site A[b]	Site B[b]
CO:				
O<u>C</u>/ZrO_2–NP	0.00	4.04	0.00	3.99
C<u>O</u>/ZrO_2–NP	4.51	7.78	4.64	8.12
NO:				
O<u>N</u>/ZrO_2–NP	0.00	2.92	0.00	2.27
N<u>O</u>/ZrO_2–NP	2.13	6.25	2.14	4.07
N_2O:				
O<u>N_2</u>/ZrO2–NP	1.17	6.82	4.53	10.12
N_2<u>O</u>/ZrO2–NP	0.00	4.22	0.00	5.22

[a] Compared with the most stable configuration, in kcal/mol.

[b] Adsorption sites, A and B are defined as centers of Zr1 and Zr3 which are shown in Figure 3.3, respectively

Adsorption energies of all studied gases on two different types of adsorption sites (A or B) on the ZrO_2–NP are shown in Table 3.4. It shows that all adsorption energies of gases adsorbed on adsorption site A of the ZrO_2–NP either obtained using the B3LYP/GEN or M06–2X/GEN computations are lower than their corresponding adsorption energies of gases adsorbed on adsorption site B. The B3LYP/GEN–adsorption abilities of the ZrO_2–NP for diatomic (H_2, N_2, O_2, CO, NO) gases on either site A or B are in the same order. The adsorption abilities for diatomic gases are in orders: O_2/ZrO_2–NP(t) (ΔE_{ads}= –43.72 kcal/mol) > O<u>C</u>/ZrO_2–NP (ΔE_{ads}= –11.45 kcal/mol) > O_2/ZrO_2–NP (ΔE_{ads}= –9.66 kcal/mol) > O<u>N</u>/ZrO_2–NP (ΔE_{ads}= –8.29 kcal/mol) > C<u>O</u>/ZrO_2–NP (ΔE_{ads}= –6.94 kcal/mol) ≈ N_2/ZrO_2–NP (ΔE_{ads}= –6.77 kcal/mol) ≈ N<u>O</u>/ZrO_2–NP (ΔE_{ads}= –6.16 kcal/mol) > H_2/ZrO_2–NP (ΔE_{ads}= –1.94 kcal/mol) for site A and O_2/ZrO_2–NP(t) (ΔE_{ads}= –41.52 kcal/mol) > O<u>C</u>/ZrO_2–NP (ΔE_{ads}= –7.41 kcal/mol) > O_2/ZrO_2–NP (ΔE_{ads}=–7.36 kcal/mol) > O<u>N</u>/ZrO_2–NP (ΔE_{ads}= –5.37 kcal/mol) > C<u>O</u>/ZrO_2–NP (ΔE_{ads}= –3.67 kcal/mol) ≈ N_2/ZrO_2–NP (ΔE_{ads}= –3.48 kcal/mol) ≈ N<u>O</u>/ZrO_2–NP (ΔE_{ads}= –2.04 kcal/mol) > H_2/ZrO_2–NP (ΔE_{ads}= –1.1 kcal/mol) for site B. Nevertheless, the adsorption abilities based on the

M06–2X/GEN calculations are in the same order of the B3LYP/GEN calculations except non–preferred adsorption orientations for N<u>O</u>, N_2 and C<u>O</u> toward Zr adsorption center.

The adsorption abilities based on the B3LYP/GEN method for triatomic (CO_2, N_2O, NO_2, H_2O, SO_2 and H_2S) gases are in orders: H_2O/ZrO_2–NP (ΔE_{ads}= –29.24 kcal/mol) > SO_2/ZrO_2–NP (ΔE_{ads}= –18.42 kcal/mol) > H_2S/ZrO_2–NP (ΔE_{ads}= –12.3 kcal/mol) > $O_2\underline{N}/ZrO_2$–NP (ΔE_{ads}= –10.06 kcal/mol) > $C\underline{O}_2/ZrO_2$–NP (ΔE_{ads}= –9.85 kcal/mol) ≈ N_2O/ZrO_2–NP (ΔE_{ads}= –9.62 kcal/mol) ≈ $O\underline{N}_2/ZrO_2$–NP (ΔE_{ads}= –8.46 kcal/mol) for site A and H_2O/ZrO_2–NP (ΔE_{ads}= –20.42 kcal/mol) > SO_2/ZrO_2–NP (ΔE_{ads}= –7.14 kcal/mol) > H_2S/ZrO_2–NP (ΔE_{ads}= –5.69 kcal/mol) ≈ $O_2\underline{N}/ZrO_2$–NP (ΔE_{ads}= –5.57 kcal/mol) ≈ N_2O /ZrO_2–NP (ΔE_{ads}= –5.4 kcal/mol) ≈ $C\underline{O}_2/ZrO_2$–NP (ΔE_{ads}= –3.97 kcal/mol) > $O\underline{N}_2/ZrO_2$–NP (ΔE_{ads}= –2.8 kcal/mol) for site B. For the adsorption abilities based on the M06–2X/GEN calculations are in different orders: $O_2\underline{N}/ZrO_2$–NP (ΔE_{ads}= –52.11 kcal/mol) > H_2O/ZrO_2–NP (ΔE_{ads}= –35.14 kcal/mol) > SO_2/ZrO_2–NP (ΔE_{ads}= –26.97 kcal/mol) > H_2S/ZrO_2–NP (ΔE_{ads}= –18.67 kcal/mol) > N_2O/ZrO_2–NP (ΔE_{ads}= –17.68 kcal/mol) > $C\underline{O}_2/ZrO_2$–NP (ΔE_{ads}= –15.51 kcal/mol) > $O\underline{N}_2/ZrO_2$–NP (ΔE_{ads}= –13.15 kcal/mol) for site A and $O_2\underline{N}/ZrO_2$–NP (ΔE_{ads}= –47.97 kcal/mol) > H_2O/ZrO_2–NP (ΔE_{ads}= –25.36 kcal/mol) > SO_2/ZrO_2–NP (ΔE_{ads}= –14.97 kcal/mol) > N_2O/ZrO_2–NP (ΔE_{ads}= –12.46 kcal/mol) > H_2S/ZrO_2–NP (ΔE_{ads}= –11.81 kcal/mol) > $C\underline{O}_2/ZrO_2$–NP (ΔE_{ads}= –10.74 kcal/mol) > $O\underline{N}_2/ZrO_2$–NP (ΔE_{ads}= –7.57 kcal/mol) for site B. Due to the M06–2X/GEN calculations, the extremely strong adsorption for $O_2\underline{N}/ZrO_2$–NP was obtained, the adsorption for $O_2\underline{N}/ZrO_2$–NP computed using other DFT methods should be investigated.

The B3LYP/GEN– and M06–2X/GEN–adsorption abilities of the ZrO_2–NP for polyatomic (C_2H_2, C_2H_4, CH_4 and NH_3) gases on either site A or B are in the same order. The adsorption abilities for polyatomic gases are in orders: NH_3/ZrO_2–NP (ΔE_{ads}= –32.73 kcal/mol) > C_2H_2/ZrO_2–NP (ΔE_{ads}= –13.77 kcal/mol) ≈ C_2H_4/ZrO_2–NP (ΔE_{ads}= –12.97 kcal/mol) > CH_4/ZrO_2–NP (ΔE_{ads}= –4.36 kcal/mol) for site A and NH_3/ZrO_2–NP (ΔE_{ads}= –23.34 kcal/mol) > C_2H_2/ZrO_2–NP (ΔE_{ads}= –6.82 kcal/mol) ≈ C_2H_4/ZrO_2–NP (ΔE_{ads}= –6.26 kcal/mol) > CH_4/ZrO_2–NP (ΔE_{ads}= –1.71 kcal/mol) for site B. For the M06–2X/GEN–adsorption abilities are in orders: NH_3/ZrO_2–NP (ΔE_{ads}= –39.88 kcal/mol) > C_2H_2/ZrO_2–NP (ΔE_{ads}= –20.34 kcal/mol) ≈ C_2H_4/ZrO_2–NP (ΔE_{ads}= –20.27

kcal/mol) > CH_4/ZrO_2–NP (ΔE_{ads}= –9.73 kcal/mol) for site A and NH_3/ZrO_2–NP (ΔE_{ads}= –29.47 kcal/mol) > C_2H_2/ZrO_2–NP (ΔE_{ads}= –12.21 kcal/mol) ≈ C_2H_4/ZrO_2–NP (ΔE_{ads}= –12.19 kcal/mol) > CH_4/ZrO_2–NP (ΔE_{ads}= –5.17 kcal/mol) for site B.

3.4 Energy gaps of the ZrO_2–NP and its adsorption complexes

The energy gaps for ZrO_2–NP and its adsorption complexes with each studied gases, computed at using the B3LYP/GEN and M06–2X/GEN methods are listed in Table A3, in Appendix. In all cases, energy gaps of all complexes computed by the M06–2X/GEN method are broader than those computed by B3LYP/GEN method. It remarkably shows that all the M06–2X/GEN–energy gap values are much overestimate; the energy gaps for ZrO_2–NP computed at using the B3LYP/GEN and M06–2X/GEN methods are 5.719 eV and 8.365 eV, respectively. The energy gap of the ZrO_2 crystal was experimentally determined to be approximately 6 eV of which the value is fundamentally independent of phase type [84]. It can remark that the structures obtained by the M06–2X/GEN method are less accurate than the B3LYP/GEN method. Therefore, all the optimized structures obtained using the B3LYP/GEN method are reliable results and reported as main feature. As energy gaps of ZrO_2–NP and its adsorption complexes with gases were obtained, it can be concluded that the zirconia nanoparticle can be used for detection of oxygen molecule via its conductivity measurement because high difference of the ZrO_2–NP (E_{gap} = 5.719 eV) and O_2/ ZrO_2–NP (E_{gap}= 1.844 and E_{gap}= 2.149 eV for adsorption on sites A and B, respectively) was found.

Table 3.4 Adsorption energies of various gases on the ZrO_2–NP of two different adsorption sites, computed at the B3LYP/GEN and M06–2X/GEN levels of theory.

Gases adsorption	ΔE_{ads},[a]			
	B3LYP/GEN		M06–2X/GEN	
	Site A[b]	Site B[b]	Site A[b]	Site B[b]
Diatomic				
H_2:				
ZrO_2–NP + H_2 → H_2/ZrO_2–NP	–1.94	–1.10	–4.18	–3.10
N_2:				
ZrO_2–NP + N_2 → N_2/ZrO_2–NP	–6.77	–3.48	–10.81	–7.57
O_2:				
ZrO_2–NP + O_2 → O_2/ZrO_2–NP	–9.66	–7.36	–12.87	–10.78
ZrO_2–NP + O_2 → O_2/ZrO_2–NP(t)[c]	–43.72	–41.52	–45.21	–43.56
CO:				
ZrO_2–NP + CO → O<u>C</u>/ZrO_2–NP	–11.45	–7.41	–15.22	–11.24
ZrO_2–NP + CO → C<u>O</u>/ZrO_2–NP	–6.94	–3.67	–10.59	–7.10
NO:				
ZrO_2–NP + NO → O<u>N</u>/ZrO_2–NP	–8.29	–5.37	–11.78	–9.51
ZrO_2–NP + NO → N<u>O</u>/ZrO_2–NP	–6.16	–2.04	–9.64	–7.71
Triatomic				
CO_2:				
ZrO_2–NP + CO_2 → CO_2/ZrO_2–NP	–9.85	–3.97	–15.51	–10.74
N_2O:				
ZrO_2–NP + N_2O → O<u>N</u>$_2$/ZrO_2–NP	–8.46	–2.80	–13.15	–7.57
ZrO_2–NP + N_2O → N_2<u>O</u>/ZrO_2–NP	–9.62	–5.40	–17.68	–12.46
NO_2:				
ZrO_2–NP + NO_2 → O_2<u>N</u>/ZrO_2–NP	–10.06	–5.57	–52.11	–47.97
H_2O:				
ZrO_2–NP + H_2O → H_2O/ZrO_2–NP	–29.24	–20.42	–35.14	–25.36
H_2S:				
ZrO_2–NP + H_2S → H_2S /ZrO_2–NP	–12.30	–5.69	–18.67	–11.81
SO_2:				
ZrO_2–NP + SO_2 → SO_2/ZrO_2–NP	–18.42	–7.14	–26.97	–14.97
Tetraatomic				
C_2H_2:				
ZrO_2–NP + C_2H_2 → C_2H_2/ZrO_2–NP	–13.77	–6.82	–20.34	–12.21
C_2H_4:				
ZrO_2–NP + C_2H_4 → C_2H_4/ZrO_2–NP	–12.97	–6.26	–20.27	–12.19
CH_4:				
ZrO_2–NP + CH_4 → CH_4/ZrO_2–NP	–4.36	–1.71	–9.73	–5.17
NH_3:				
ZrO_2–NP + NH_3 → H_3<u>N</u>/ZrO_2–NP	–32.73	–23.34	–39.88	–29.47

[a] In kcal/mol.

[b] Adsorption sites, A and B are defined as centers of Zr1 and Zr3 which are shown in Figure 3.3, respectively

[c] Oxygen molecule is treated as triplet state.

3.5 Structures of the C_{2v} symmetry $(ZrO_2)_{12}$ cluster doped by single metal atoms

The structures of zirconia nanoparticle (ZrO_2–NP) doped by single atom of metal M which denoted by M–ZrO_2–NP shown in Figure 3.7 are defined and compared with non–doped zirconia nanoparticle. The structure optimizations for the M–doped $(ZrO_2)_{12}$ clusters were carried out using DFT B3LYP and M06–2X methods. The B3LYP/GEN–optimized structures for the ZrO_2–NP are shown in Figure 3.8. The selected geometrical parameters for M–ZrO_2–NP clusters computed at the B3LYP/GEN method are shown in Table 3.5.

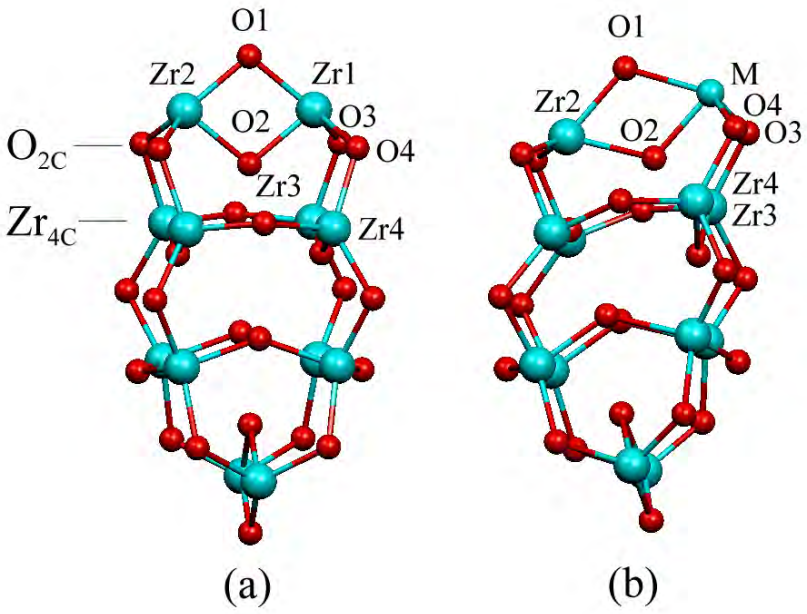

Figure 3.7 The structure of (a) zirconia nanoparticle (ZrO_2–NP), represented as the most stable $(ZrO_2)_{12}$ cluster and (b) its structure doped by single atom of metal M which denoted by M–ZrO_2–NP.

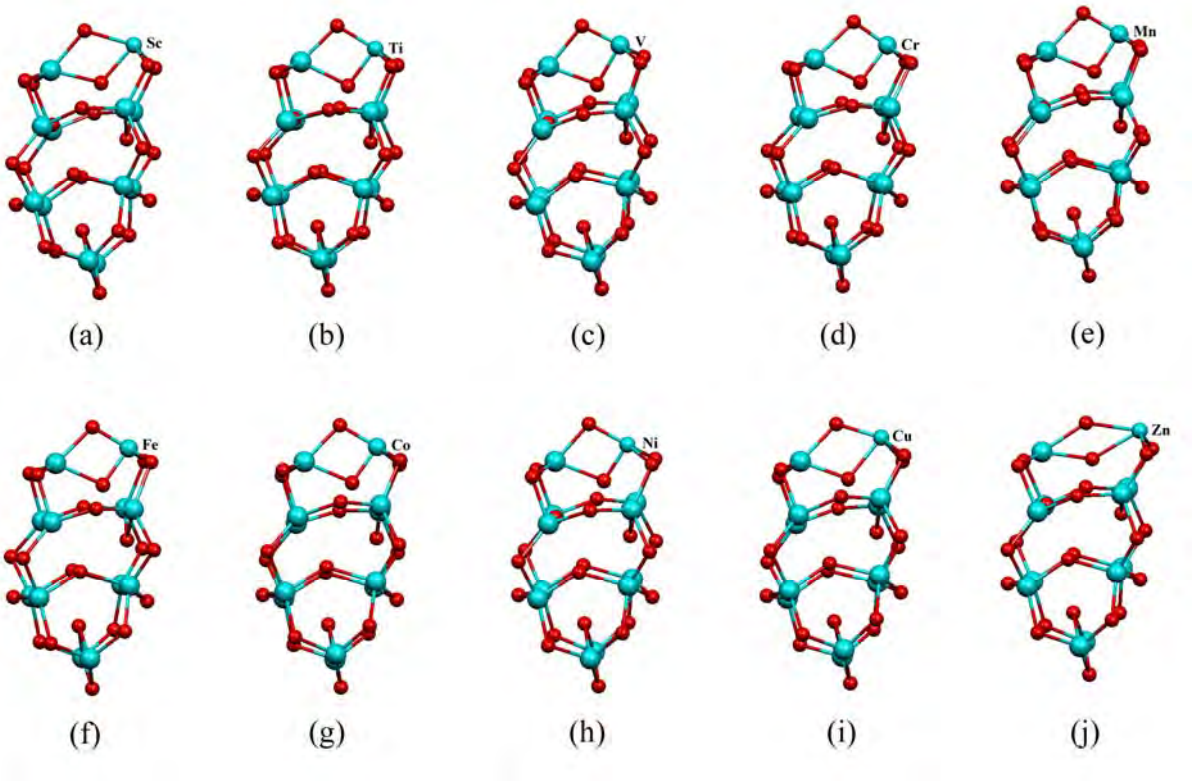

Figure 3.8 M–doped ZrO_2–NP as (a) Sc–doped ZrO_2–NP, (b) Ti–doped ZrO_2–NP, (c) V–doped ZrO_2–NP, (d) Cr–doped ZrO_2–NP, (e) Mn–doped ZrO_2–NP, (f) Fe–doped ZrO_2–NP, (g) Co–doped ZrO_2–NP, (h) Ni–doped ZrO_2–NP, (i) Cu–doped ZrO_2–NP and (j) ZN–doped ZrO_2–NP.

Table 3.5 Geometrical parameters for ZrO_2–NP, its metal doped clusters and hydrogen gas adsorption structures, computed at the B3LYP/GEN method.

M–ZrO_2–NPs	Non–	Sc–	Ti–	V–	Cr–	Mn–	Fe–	Co–	Ni–	Cu–	Zn–
Bond length [a]											
O1–M	2.03	2.11	1.82	1.74	1.68	1.70	1.73	1.77	1.79	1.92	2.23
O2–M	2.03	2.04	1.88	1.87	1.87	1.84	1.83	1.79	1.77	2.18	2.28
O1–Zr2	2.03	2.14	2.08	2.16	2.23	2.17	2.13	2.09	2.08	2.12	2.18
Bond angle [b]											
O1–M–O2	79.30	65.06	84.24	86.43	88.21	86.64	85.01	85.49	85.40	68.41	39.12
O1–M–O3	126.67	119.45	124.81	126.65	128.11	125.86	123.69	129.63	134.65	128.05	105.40
O1–M–O4	126.67	119.48	124.81	126.65	128.11	125.86	123.69	129.63	134.65	128.05	105.40
O3–M–O4	106.17	106.49	109.07	106.01	103.51	108.02	112.38	100.48	90.31	93.20	121.52
M–O3–Zr3	113.00	107.86	105.07	104.96	104.61	104.03	103.20	104.10	104.33	106.96	109.28
M–O4–Zr4	113.00	107.86	105.07	104.96	104.61	104.03	103.20	104.10	104.33	106.96	109.28
H_2 adsorption											
Bond distance [c]											
[M···H_2]	2.78	2.65	2.61	2.44	2.24	2.18	2.13	2.15	2.14	2.71	2.49
Angle [b]											
O1–M–H	81.29	88.03	82.64	93.85	91.95	92.39	81.12	92.86	80.46	89.07	102.57
Dihedral angle [b]											
O1–M–H–H	–179.99	178.58	179.86	–90.71	–90.40	–90.48	–178.94	–88.70	–179.99	–179.93	–92.66

[a] In Å.

[b] In degree.

[c] Hydrogen bond distance, in Å.

3.6 Energy gaps of M–ZrO_2–NP clusters

HOMO, LUMO energies and energy gaps of ZrO_2–NP and M–ZrO_2–NP clusters computed using B3LYP method are shown in Table 3.6; these values computed using M06–2X method are shown in Table A4, in Appendix. As the energy gap for the ZrO_2–NP (E_{gap} = 5.719 eV) derived from the B3LYP method is close to the experimental band gap of ZrO_2 crystals ($E_{gap} \approx$ 6.0 eV) as compared with the value (E_{gap} = 8.365 eV) obtained from the M06–2X method, the energy gaps computed by B3LYP method have only been mentioned otherwise specified. Table 3.6 shows that energy gaps for all the M–doped ZrO_2–NP clusters are obviously much more narrow the non–doped ZrO_2–NP. Plot of energy gaps of non– and M–doped ZrO_2–NPs against their atomic numbers is shown in Figure 3.9. It shows that energy gap of Cu–doped ZrO_2–NP is the lowest value. The magnitudes of energy gaps for M–doped ZrO_2–NP clusters are in decreasing order: Sc–doped (E_{gap} = 5.181 eV) > Ti–doped (E_{gap} = 5.144 eV) > Zn–doped (E_{gap} = 4.957 eV) > Mn–doped (E_{gap} = 3.669 eV) > V–doped (E_{gap} = 3.513 eV) > Fe–doped (E_{gap} = 3.506 eV) > Co–doped (E_{gap} = 3.109 eV) > Ni–doped (E_{gap} = 2.788 eV) > Cr–doped (E_{gap} = 2.760 eV) > Cu–doped (E_{gap} = 1.993 eV). The biggest change ($\Delta E_g \approx$ 65 %) in energy gap compared with the non–doped ZrO_2–NP is the Cu–doped ZrO_2–NP. This means that the Cu–doped ZrO_2–NP is the most reactive species which has potential to adsorb adsorbate gases.

Due to all the M06–2X–energy gaps are less accurate than those computed using the B3LYP method, their values are therefore less important to be presented.

3.7 Adsorptions of single molecules of gases on the ZrO_2–NP

The structures of adsorption configurations of hydrogen gas adsorbed on metal atom of the M–doped ZrO_2–NPs are shown in Figure 3.10 and their adsorption energies are shown in Table 3.7. The adsorption abilities for hydrogen gas of M–doped ZrO_2–NPs are in order: Cu–doped (ΔE_{ads} = –5.16 kcal/mol) > Cr–doped (ΔE_{ads} = –2.87 kcal/mol) > Mn–doped (ΔE_{ads} = –2.74 kcal/mol) > Fe–doped (ΔE_{ads} = –2.68 kcal/mol) > V–doped (ΔE_{ads} = –2.45 kcal/mol) > Sc–doped (ΔE_{ads} = –2.40 kcal/mol) > Ti–doped

(ΔE_{ads} = –2.21 kcal/mol) > Ni–doped (ΔE_{ads} = –2.19 kcal/mol) > Co–doped (ΔE_{ads} = –2.12 kcal/mol) > Zn–doped (ΔE_{ads} = –1.72 kcal/mol). As adsorption energies of M–doped ZrO_2–NPs compared with non–doped ZrO_2–NP (ΔE_{ads} = –1.94 kcal/mol), the Zn doping in Zn–doped ZrO_2–NP does not enhance for hydrogen gas adsorption. Plot of adsorption energy for hydrogen gas adsorbed on non– and M–doped ZrO2–NPs against their atomic numbers are presented in Figure 3.11. It shows that the Cu doping in Cu–doped ZrO_2–NP significantly improve for hydrogen gas adsorption. Their adsorption energies for hydrogen gas are listed in Table 3.7.

Nevertheless, adsorption structures for hydrogen were optimized at the M06–2X/GEN method but optimization for structures of H_2/Sc–, H_2/Cr–, H_2/Mn–, H_2/Co–, H_2/Ni– and H_2/Cu–doped ZrO_2–NPs have never been carried out. Therefore, the adsorption energies computed at the M06–2X/GEN//B3LYP/GEN were tested but it seems to be that these values are inaccurate as shown in Table A5, in Appendix.

Table 3.6 Energies of frontier orbitals and energy gaps of ZrO_2–NP doped by single metal atom, computed at two different levels of theory.

Metal–doped ZrO_2–NPs	E_{HOMO}[a]	E_{LUMO}[a]	E_{gap}[a]	ΔE_{gap},[b]
Non–doped	–7.903	–2.184	5.719	–
Sc–doped	–7.722	–2.541	5.181	9.41
Ti–doped	–7.805	–2.661	5.144	10.05
V–doped	–6.727	–3.214	3.513	38.57
Cr–doped	–6.384	–3.624	2.760	51.74
Mn–doped	–7.231	–3.562	3.669	35.85
Fe–doped	–7.361	–3.855	3.506	38.70
Co–doped	–7.763	–4.653	3.109	45.63
Ni–doped	–7.870	–5.081	2.788	51.24
Cu–doped	–7.914	–5.921	1.993	65.15
Zn–doped	–7.598	–2.642	4.957	13.33

[a] In eV.

[b] Difference between energy gaps of metal– and non–doped ZrO_2–NPs, in %.

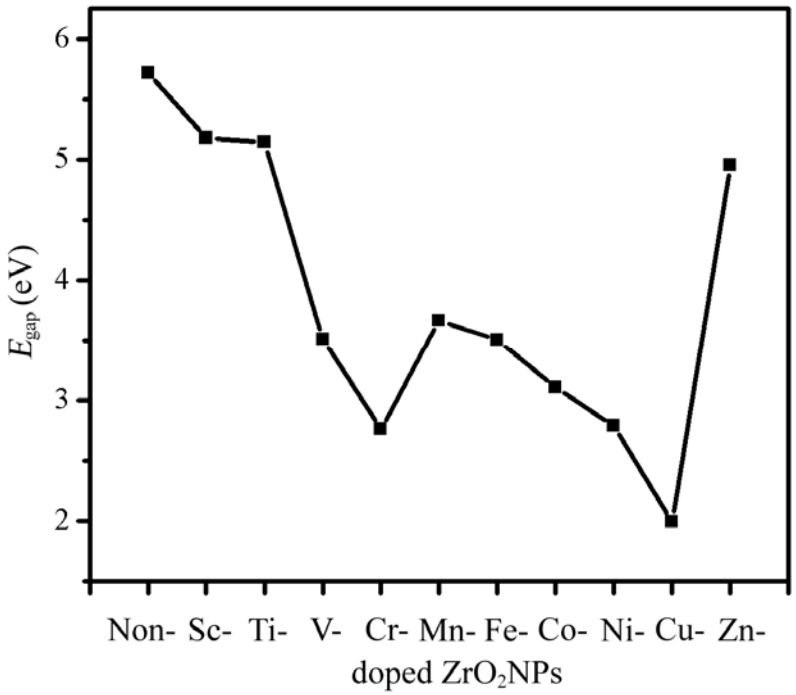

Figure 3.9 Plot of energy gaps of non– and M–doped ZrO_2–NPs against their atomic numbers.

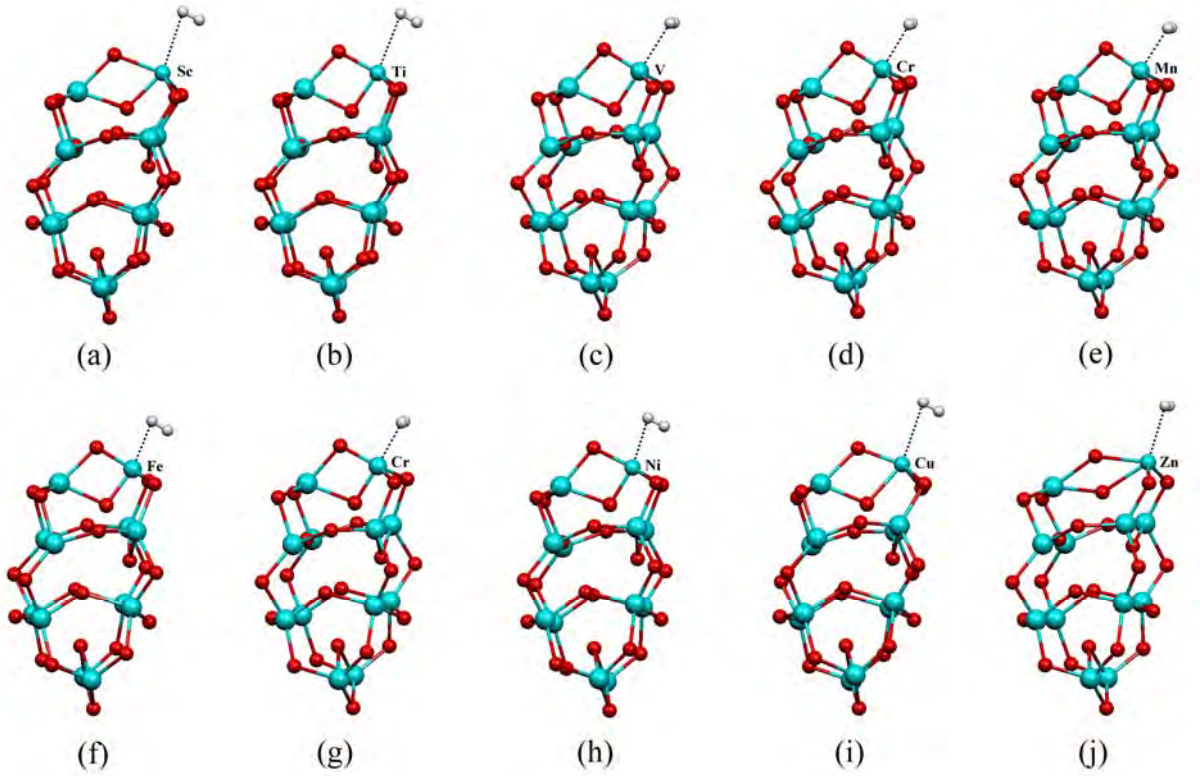

Figure 3.10 Hydrogen gas adsorption structures as (a) H_2/Sc–doped ZrO_2–NP, (b) H_2/Ti–doped ZrO_2–NP, (c) H_2/V–doped ZrO_2–NP, (d) H_2/Cr–doped ZrO_2–NP, (e) H_2/Mn–doped ZrO_2–NP, (f) H_2/Fe–doped ZrO_2–NP, (g) H_2/Co–doped ZrO_2–NP, (h) H_2/Ni–doped ZrO_2–NP, (i) H_2/Cu–doped ZrO_2–NP and (j) H_2/ZN–doped ZrO_2–NP.

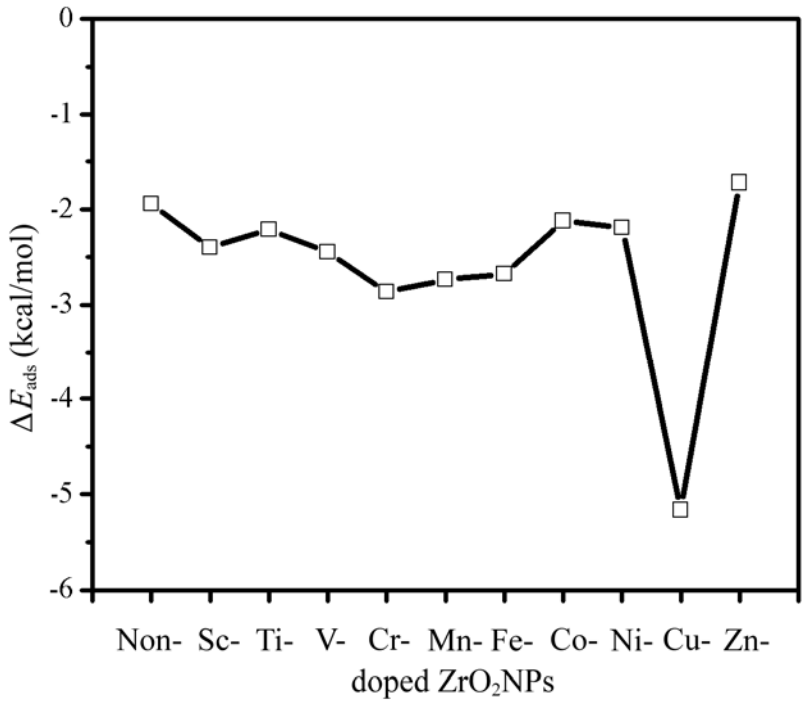

Figure 3.11 Plot of adsorption energy for hydrogen gas adsorbed on non– and M–doped ZrO_2–NPs against their atomic numbers.

Table 3.7 Adsorption energies of hydrogen gas on metal–doped ZrO_2–NPs compared with non–doped ZrO_2–NP, computed at the B3LYP/GEN level of theory.

H_2 adsorbed on M–doped ZrO_2–NPs	ΔE_{ads} [a]
H_2/non–doped	–1.94
H_2/Sc–doped	–2.40
H_2/Ti–doped	–2.21
H_2/V–doped	–2.45
H_2/Cr–doped	–2.87
H_2/Mn–doped	–2.74
H_2/Fe–doped	–2.68
H_2/Co–doped	–2.12
H_2/Ni–doped	–2.19
H_2/Cu–doped	–5.16
H_2/Zn–doped	–1.72

[a] In kcal/mol.

CHAPTER IV

CONCLUSIONS

The adsorption of CO and NH_3 gases on the cubic ZrO_2 (110) surface was investigated by two–dimensionally periodic slab model DFT calculations. The adsorption energies of NH_3 on the cubic ZrO_2 (110) surface are –27.62 and –25.51 kcal/mol, obtained using the PBE0 and B3LYP methods, respectively. The CO adsorption on the cubic ZrO_2 (110) surface –11.39 and –9.81 kcal/mol, obtained using the PBE0 with rigid and flexible models, respectively.

The adsorption configurations of diatomic (H_2, N_2, O_2, CO and NO), triatomic (CO_2, N_2O, NO_2, H_2O, SO_2 and H_2S) and polyatomic (C_2H_2, C_2H_4, CH_4 and NH_3) gases on the zirconia nanoparticle (ZrO_2–NP), represented by the high symmetric $(ZrO_2)_{12}$ cluster were studied using the B3LYP and M06–2X methods. Energy gaps of all complexes computed by the M06–2X/GEN method are much broader than those computed by B3LYP/GEN method. It remarks that the ZrO_2–NP structure and its adsorption complexes obtained by the M06–2X/GEN method are less accurate than the B3LYP/GEN. Adsorptions of all relevant gases on the ZrO_2–NP can be concluded as follows.

(1) Relative energies either obtained from the B3LYP/GEN or M06–2X/GEN methods result that stabilities of these three pairs of adsorption configurations are in orders: O<u>C</u>/ZrO_2–NP(A) > O<u>C</u>/ZrO_2–NP(B) > C<u>O</u>/ZrO_2–NP(A) > C<u>O</u>/ZrO_2–NP(B), O<u>N</u>/ZrO_2–NP(A) > N<u>O</u>/ZrO_2–NP(A) > O<u>N</u>/ZrO_2–NP(B) > N<u>O</u>/ZrO_2–NP(B) and N_2<u>O</u>/ZrO2–NP(A) > O<u>N_2</u>/ZrO2–NP(A) > N_2<u>O</u>/ZrO2–NP(B) > O<u>N_2</u>/ZrO2–NP(B).

(2) All adsorption energies of gases adsorbed on adsorption site A of the ZrO_2–NP either obtained using the B3LYP/GEN or M06–2X/GEN computations are lower than their corresponding adsorption energies of gases adsorbed on adsorption site B.

(3) The B3LYP/GEN–adsorption abilities of the ZrO_2–NP for diatomic (gases on either site A or B are in the same order: O_2/ZrO_2–NP(t) > O<u>C</u>/ZrO_2–NP > O_2/ZrO_2–NP > O<u>N</u>/ZrO_2–NP > C<u>O</u>/ZrO_2–NP ≈ N_2/ZrO_2–NP ≈ N<u>O</u>/ZrO_2–NP > H_2/ZrO_2–NP.

(4) The adsorption abilities based on the B3LYP/GEN method for triatomic (CO_2, N_2O, NO_2, H_2O, SO_2 and H_2S) gases are in orders: H_2O/ZrO_2–NP > SO_2/ZrO_2–NP > H_2S/ZrO_2–NP > $O_2\underline{N}/ZrO_2$–NP > $C\underline{O}_2/ZrO_2$–NP ≈ N_2O/ZrO_2–NP ≈ $O\underline{N}_2/ZrO_2$–NP for site A and H_2O/ZrO_2–NP > SO_2/ZrO_2–NP > H_2S/ZrO_2–NP ≈ $O_2\underline{N}/ZrO_2$–NP ≈ N_2O/ZrO_2–NP ≈ $C\underline{O}_2/ZrO_2$–NP > $O\underline{N}_2/ZrO_2$–NP for site B.

(5) The B3LYP/GEN– and M06–2X/GEN–adsorption abilities of the ZrO_2–NP for polyatomic (C_2H_2, C_2H_4, CH_4 and NH_3) gases on either site A or B are in the same order: NH_3/ZrO_2–NP > C_2H_2/ZrO_2–NP ≈ C_2H_4/ZrO_2–NP > CH_4/ZrO_2–NP.

(6) As energy gaps of ZrO_2–NP and its adsorption complexes with gases were obtained, it can be concluded that the zirconia nanoparticle can be used for detection of oxygen molecule via its conductivity measurement because high difference of the ZrO_2–NP (E_{gap} = 5.719 eV) and O_2/ ZrO_2–NP (E_{gap}= 1.844 eV and E_{gap}= 2.149 eV for adsorption on sites A and B, respectively) was found.

The structure optimizations for the M–doped $(ZrO_2)_{12}$ clusters were carried out using DFT B3LYP and M06–2X methods. Their energy gaps were obtained and it found that the B3LYP-energy gap of ZrO_2–NP is more accurate than the obtained from the M06–2X method. The magnitudes of energy gaps for M–doped ZrO_2–NP clusters are in decreasing order: Sc–doped (E_{gap} = 5.181 eV) > Ti–doped (E_{gap} = 5.144 eV) > Zn–doped (E_{gap} = 4.957 eV) > Mn–doped (E_{gap} = 3.669 eV) > V–doped (E_{gap} = 3.513 eV) > Fe–doped (E_{gap} = 3.506 eV) > Co–doped (E_{gap} = 3.109 eV) > Ni–doped (E_{gap} = 2.788 eV) > Cr–doped (E_{gap} = 2.760 eV) > Cu–doped (E_{gap} = 1.993 eV). The Cu–doped ZrO_2–NP was found to be the most reactive species and has potential to adsorb adsorbate gases.

The adsorption abilities for hydrogen gas of M–doped ZrO_2–NPs are in order: Cu–doped > Cr–doped > Mn–doped > Fe–doped > V–doped > Sc–doped > Ti–doped > Ni–doped > Co–doped (ΔE_{ads} = –2.12 kcal/mol) > Zn–doped. The Zn doping in Zn–doped ZrO_2–NP does not enhance for hydrogen gas adsorption. The Cu doping in Cu–doped ZrO_2–NP significantly improve for hydrogen gas adsorption.

REFERENCES

[1] J. Miller, S. Rankin, E. Ko, J. Catal. 148 (1994) 673–683.

[2] E. M. Köck, M. Kogler, T. Bielz, B. Klötzer, S. Penner, J. Phys.Chem. C 117 (2013) 17666−17673.

[3] T. M. Miller, V. H. Grassian, Catal. Lett. 46 (1997) 213−221.

[4] Q. Zhao, The thermal stability and catalytic application of MnO_x–ZrO_2 Oxide Powders, Diss. Drexel University, 2004.

[5] I. Matsukuma, S. Kikuyama, R. Kikuchi, K. Sasaki, K. Eguchi, Appl. Catal. B 37 (2002) 107–115.

[6] K. Eguchi, M. Watabe, S. Ogata, H. Arai, Bull. Chem. Soc. Jpn. 68 (1995) 1739–1745.

[7] K. Eguchi, M. Watabe, S. Ogata, H. Arai, J. Catal. 158 (1996) 420–426.

[8] M.J. Poston, A.B. Aleksandrov, D.E. Sabo, Z.–J. Zhang, T.M. Orlando, J. Phys. Chem. C 118 (2014) 12789−12795.

[9] M. Kogler, E.–M. Köck, Th. Bielz, K. Pfaller, B. Klötzer, D. Schmidmair, L. Perfler, S. Penner, J. Phys. Chem. C 118 (2014) 8435−8444.

[10] K. Sayama, H. Arakawa, Catalyst. J. Phys. Chem. 1993, 97, 531−533.

[11] Y. Cao, R. Ran, X. Wu, B. Zhao, J. Wan, D. Weng, Appl. Catal. A 457 (2013) 52–61.

[12] X. Wu, H. Lee, S. Liu, D. Weng, J. Rare Earths 30 (2012) 659–664.

[13] I. Atribak, I. Such–Basáñez, A. Bueno–López, J. Catal. 250 (2007) 75–84.

[14] M.G. Cutrufello, I. Ferino, V. Solinas, A. Primavera, A. Trovarelli, A. Auroux, C. Picciau, Phys. Chem. Chem. Phys. 1 (1999) 3369–3375.

[15] K. T. Jung and A. T. Bell, J. Catal., 2001, 204, 339–347.

[16] D. Sato, D. Meira, S. Damyanova, E. Longo, J. Bueno, J. Catal. 307 (2013) 1–17.

[17] K. Tanabe, Mater. Chem. Phys. 13 (1985) 347–364.

[18] K. Jung, A. Bell, J. Mol. Catal. A: Chem. 163 (2000) 27–42.

[19] L. Chen, S. Wang, J. Zhou, Y. Shen, Y. Zhao, X. Ma, RSC Adv., 4 (2014) 30968–30975.

[20] K.J. Puolaakka, S. Juutilainen, O. Krause, Catal. Today 115 (2006) 217–221.

[21] H. Rönkkönen, E. Rikkinen, J. Linnekoski, P. Simell, M. Reinikainen, O. Krause, Catal. Today 147S (2009) S230–S236.

[22] S. Juutilainen, P. Simell, O. Krause, Doped zirconias in catalytic clean–up of gasification gas, in: A.V. Bridgwater, D.G.B. Boocock (Eds.), Sciences of Thermal and Chemical Biomass Conversion, vol. 1, CPL Press, 2006.

[23] S. Juutilainen, P. Simell, O. Krause, Appl. Catal. B 62 (2006) 86–92.

[24] T. Viinikainen, H. Rönkkönen, H. Bradshaw, H. Stephenson, S. Airaksinen, M. M. Reinikainen, P. Simell, O. Krause, Appl. Catal. A 362 (2009) 169–177.

[25] H. Rönkkönen, P. Simell, M. Reinikainen, O. Krause, Top. Catal. 52 (2009) 1070–1078.

[26] H.H. Kung, Stud. Surf. Sci. Catal. 45 (1989) 200–226.

[27] K. Tanabe, T. Yamaguchi, Catal. Today 20 (1994) 185–198.

[28] J.N. Harvey, M. Diefenbach, D. Schröder, H. Schwarz, Int. J. Mass Spectrom. 182/183 (1999) 85–97.

[29] A. Corma, Chem. Rev. 95 (1995) 559–614.

[30] D.A. Ward, E.I. Ko, Chem. Mater. 5 (1993) 956–969.

[31] S. Heinbuch, F. Dong, J.J. Rocca, E.R. Bernstein, J. Opt. Soc. Am. B 25 (2008) B85–B91.

[32] S. Chretien, H.J. Metiu, Chem. Phys. 127 (2007) 244708.

[33] S. Chretien, H.J. Metiu, Chem. Phys. 128 (2008) 044714.

[34] S. Chretien, H.J. Metiu, Chem. Phys. 129 (2008) 074705.

[35] J.G. Bendoraitis, R.E. Salomon, J. Phys. Chem. 69 (1965) 3666–3667.

[36] J.–M. Herrmann, J. Disdier, P. Pichat, J. Chem. Soc. Faraday Trans. 1 77(11) (1981) 2815–2826.

[37] S. Sato, T. Kadowaki, J. Catal. 106 (1987) 295–300.

[38] A.R. Newmark, U. Stimming, Langmuir 3 (1987) 905–910.

[39] H. Wiemhöfer, U. Voher, Ber. Bunsenges Phys. Chem. 96 (1992) 1646–1652.

[40] K. Ganguly, S. Sarkar, S. Bhattacharyya, J. Chem. Soc. Chem. Comm. (1993) 682–683.

[41] S. Preusser, U. Stimming, K. Wippermann, Electrochim. Acta 39 (1994) 1273–1280.

[42] R.H. French, S.J. Glass, F.S. Ohuchi, Y.N. Xu, W.Y. Ching, Phys. Rev. B 49 (1994) 5133−5141.

[43] J.A. Navío, G. Colón, Stud. Surf. Sci. Catal. 82 (1994) 721–728.

[44] D.W. McComb, Phys. Rev. B 54 (1996) 7094−7102.

[45] L. K. Dash, N. Vast, P. Baranek, M.C. Cheynet, L. Reining, Phys. Rev. B 70 (2004) 245116.

[46] M.V. Ganduglia–Pirovano, A. Hofmann, J. Sauer, Surf. Sci. Rep. 62 (2007) 219−270.

[47] A. Hofmann, S.J. Clark, M. Oppel, I. Hahndorf, Phys. Chem. Chem. Phys. 4 (2002) 3500–3508.

[48] S.–G. Li, David A. Dixon, J. Phys. Chem. A 114 (2010) 2665–2683.

[49] R. Jin, S. Zhang, Y. Zhang, S. Huang, P. Wang, H. Tian, Int. J. hydrogen energy 36 (2011) 9069–9078.

[50] O. Syzgantseva, M. Calatayud, C. Minot, Chem. Phys. Letts. 503 (2011) 12–17.

[51] A. Debernardi, D. Sangalli, A. Lamperti, E. Cianci, P. Lupo, F. Casoli, F. Albertini, L. Nasi, R. Ciprian, P. Torelli, J. Appl. Phys. 115 (2014) 17D718.

[52] D. Sangalli, E. Cianci, A. Lamperti, R. Ciprian, F. Albertini, F. Casoli, P. Lupo, L. Nasi, M. Campanini, A. Debernardi, Eur. Phys. J. B 86 (2013) 211.

[53] N.H. Hong, C.–K. Park, A.T. Raghavender, O. Ciftja, N.S. Bingham, M.H. Phan, H. Srikanth, J. Appl. Phys. 111, (2012) 07C302.

[54] J.M.D. Coey, M. Venkatesan, P. Stamenov, C.B. Fitzgerald, L.S. Dorneless, Phys. Rev. B 72 (2005) 024450.

[55] T.R. Sahoo, S.S. Manoharan, S. Kurian, N.S. Gajhiye, Hyperfine Interac. 188 (2009) 43–49.

[56] V.V. Kriventsov, D.I. Kochubey, Y.V. Maximov, I.P. Suzdalev, M.V. Tsodikov, J.A. Navio, M.C. Hidalgo, G. Colón, Nucl. Instrum. Meth. Phys. Res. A 470 (2001) 341–346.

[57] S. Ostanin, A. Ernst, L.M. Sandratskii, P. Bruno, M. Däne, I.D. Hughes, J.B. Staunton, W. Hergert, I. Mertig, J. Kudrnovskỳ, Phys. Rev. Lett. 98 (2007) 016101.

[58] T. Archer, C.D. Pemmaraju, S. Sanvito, J. Magn. Magn. Mater. 316 (2007) e188.

[59] H. R. Chauke, P. Murovhi, P.E. Ngoepe, N.H. de Leeuw, R. Grau–Crespo, J. Phys. Chem. C 114 (2010) 15403–15409.

[60] K. Samson, M. Śliwa, R. P. Socha, K. Góra–Marek, D. Mucha, D. Rutkowska–Zbik, J–F. Paul, M. Ruggiero–Mikołajczyk, R. Grabowski, J. Słoczyń ski, ACS Catal. 4 (2014) 3730−3741.

[61] R. Dovesi, V.R. Saunders, C. Roetti, R. Orlando, C.M. Zicovich–Wilson, F. Pascale, B. Civalleri, K. Doll, N.M. Harrison, I.J. Bush, P. D'Arco, M. Llunell, CRYSTAL06 User's Manual, University of Torino, Torino, 2006.

[62] G. Sophia, P. Baranek, C. Sarrazin, M. Rerat, R. Dovesi, Phase Transitions: A Multinational Journal, 2013 81 1069–1084.

[63] M.D. Towler, N.L. Allan, N.M. Harrison, V.R. Saunders, W.C. Mackrodt, E. Apra, Phys. Rev. B 50 (1994) 5041.

[64] M. Catti, A. Pavese, R. Dovesi, V.C. Saunders, J. Phys. Rev. B 47 (1993) 9189.

[65] L. Valenzano, F.J. Torres, K. Doll, F. Pascale, C.M. Zicovich–Wilson, R.Z. Dovesi, Phys. Chem. 220 (2006) 893.

[66] C. Gatti, V.R. Saunders, C. Roetti, J. Chem. Phys. 101 (1994) 10686.

[67] C. Lee, W. Yang, R.G. Parr, Phys. Rev. B 37 (1988) 785.

[68] J. P. Perdew, K. Burke, and M. Ernzerhof, Phys. Rev. Lett., 77 (1996) 3865–3868.

[69] J. P. Perdew, K. Burke, and M. Ernzerhof, Phys. Rev. Lett., 78 (1997) 1396.

[70] C. Adamo and V. Barone, J. Chem. Phys., 110 (1999) 6158–6169.

[71] D. I. Bilc, R. Orlando, R. Shaltaf, G.–M. Rignanese, J. Íñiguez, and Ph. Ghosez, Phys. Rev. B 77 (2008) 165107.

[72] J. Perdew, J. Chevary, S. Vosko, K. Jackson, M. Pederson, D. Singh, C. Fiolhais, Phys Rev B 1992, 46, 6671.

[73] U. Martin, H. Boysen, F. Frey, Acta Crystallographica Section B 49 (1993) 403–413.

[74] H.J. Monkhorst, J.D. Pack, Phys. Rev. B 13 (1976) 5188.

[75] V.G. Zavodinsky and A.N. Chibisov, Phys. Solid State 48 (2006) 343–347.

[76] A.D. Becke, J. Chem. Phys. 98 (1993) 5648–5652.

[77] C. Lee, W. Yang, R.G. Parr, Phys. Rev. B 37 (1988) 785–789.

[78] Y. Zhao, D. G. Truhlar, Theor. Chem. Acc. 120 (2008) 215–41.

[79] P.J. Hay, W.R. Wadt, J. Chem. Phys. 82 (1985) 270–283.

[80] W.R. Wadt, P.J. Hay, J. Chem. Phys. 82 (1985) 284–298.

[81] P.J. Hay, W.R. Wadt, J. Chem. Phys. 82 (1985) 299–310.

[82] R. Ditchfield, W. J. Hehre, J. A. Pople, J. Chem. Phys. 54 (1971) 724–728.

[83] M. J. Frisch, et al., Gaussian 09, Revision A.02, Gaussian, Inc., Wallingford, CT, 2009.

[84] R.H. French, S. J. Glass, F. S. Ohuchi, Y.N. Xu, W.Y. Ching, Phys. Rev. B, 49 (1994) 5133 –5142.

APPENDIX A

Table A1 B3LYP–optimized structures of ZrO_2–NPs as $(ZrO_2)_n$, n=1 to 12, and their energetics.

ZrO_2–NPs	E_{total} [a]	E_{OF} [b,c]	E_{FPU} [b,d]	ΔE_{rel} [b,e]
ZrO_2	–197.0527840			
$(ZrO_2)_2$				
$(ZrO_2)_2$_a	–394.2888882	–115.04	–57.52	6.56
$(ZrO_2)_2$_b	–394.2993398	–121.59	–60.80	0.00
$(ZrO_2)_2$_c	–394.2825328	–111.05	–55.52	10.55
$(ZrO_2)_3$				
$(ZrO_2)_3$_a	–591.5458011	–243.13	–81.04	0.00
$(ZrO_2)_3$_b	–591.5361898	–237.10	–79.03	6.03
$(ZrO_2)_3$_c	–591.5327215	–234.92	–78.31	8.21
$(ZrO_2)_3$_d	–591.4939847	–210.61	–70.20	32.52
$(ZrO_2)_3$_e	–591.5058870	–218.08	–72.69	25.05
$(ZrO_2)_4$				
$(ZrO_2)_4$_a	–788.8017645	–370.63	–92.66	0.00
$(ZrO_2)_4$_b	–788.7692489	–350.22	–87.56	20.40
$(ZrO_2)_4$_c	–788.7702703	–350.86	–87.72	19.76
$(ZrO_2)_4$_d	–788.7668101	–348.69	–87.17	21.93
$(ZrO_2)_4$_e	–788.7429330	–333.71	–83.43	36.92
$(ZrO_2)_5$				
$(ZrO_2)_5$_a	–986.0882361	–517.27	–103.45	5.55
$(ZrO_2)_5$_b	–986.0643688	–502.29	–100.46	20.53
$(ZrO_2)_5$_c	–986.0176037	–472.94	–94.59	49.87
$(ZrO_2)_5$_d	–985.9599064	–436.74	–87.35	86.08
$(ZrO_2)_5$_e	–986.0071463	–466.38	–93.28	56.44
$(ZrO_2)_5$_f	–986.0970841	–522.82	–104.56	0.00
$(ZrO_2)_5$_g	–985.9971573	–460.11	–92.02	62.71
$(ZrO_2)_6$				
$(ZrO_2)_6$_a	–1183.3663311	–658.65	–109.78	0.00
$(ZrO_2)_6$_b	–1183.3448989	–645.20	–107.53	13.45
$(ZrO_2)_6$_c	–1183.3363537	–639.84	–106.64	18.81
$(ZrO_2)_6$_d	–1183.3129385	–625.15	–104.19	33.50
$(ZrO_2)_6$_e	–1183.2442719	–582.06	–97.01	76.59
$(ZrO_2)_6$_f	–1183.2443140	–582.08	–97.01	76.57
$(ZrO_2)_6$_g	–1183.3293132	–635.42	–105.90	23.23

[a] In au. [b] In kcal/mol.
[c] Overall formation energy (E_{OF}) defined as $E_{total}(ZrO_2)_n - n\,E_{total}(ZrO_2)$.
[d] Formation energy per unit of (ZrO_2) (E_{FPU}) defined as $[E_{total}(ZrO_2)_n - n\,E_{total}(ZrO_2)]/n$.
[e] Energy related to the most stable cluster.

Table A1 Continued.

ZrO_2–NPs	E_{Total} [a]	E_{OF} [b,c]	E_{FPU} [b,d]	ΔE_{rel} [b,e]
$(ZrO_2)_7$				
$(ZrO_2)_7$_a	–1380.619226	–784.22	–112.03	19.58
$(ZrO_2)_7$_b	–1380.650426	–803.80	–114.83	0.00
$(ZrO_2)_7$_c	–1380.650299	–803.72	–114.82	0.08
$(ZrO_2)_8$				
$(ZrO_2)_8$_a	–1577.925957	–943.58	–117.95	6.82
$(ZrO_2)_8$_b	–1577.936824	–950.40	–118.80	0.00
$(ZrO_2)_8$_c	–1577.918790	–939.08	–117.39	11.32
$(ZrO_2)_8$_d	–1577.917539	–938.30	–117.29	12.10
$(ZrO_2)_8$_e	–1577.922616	–941.48	–117.69	8.92
$(ZrO_2)_9$				
$(ZrO_2)_9$_a	–1775.211839	–1089.85	–121.09	136.07
$(ZrO_2)_9$_b	–1775.201317	–1083.25	–120.36	142.68
$(ZrO_2)_9$_c	–1775.428684	–1225.92	–136.21	0.00
$(ZrO_2)_{10}$				
$(ZrO_2)_{10}$_a	–1972.513537	–1246.04	–124.60	17.37
$(ZrO_2)_{10}$_b	–1972.541215	–1263.41	–126.34	0.00
$(ZrO_2)_{10}$_c	–1972.538808	–1261.90	–126.19	1.51
$(ZrO_2)_{10}$_d	–1972.490224	–1231.42	–123.14	32.00
$(ZrO_2)_{11}$				
$(ZrO_2)_{11}$_a	–2169.757597	–1366.07	–124.19	15.51
$(ZrO_2)_{11}$_b	–2169.782316	–1381.58	–125.60	0.00
$(ZrO_2)_{11}$_c	–2169.763849	–1370.00	–124.55	11.59
$(ZrO_2)_{12}$				
$(ZrO_2)_{12}$_a	–2367.084292	–1537.95	–128.16	13.55
$(ZrO_2)_{12}$_b	–2367.105879	–1551.50	–129.29	0.00
$(ZrO_2)_{12}$_c	–2367.068746	–1528.20	–127.35	23.30
$(ZrO_2)_{12}$ d	–2367.089861	–1541.45	–128.45	10.05

[a] In au. [b] In kcal/mol.

[c] Overall formation energy (E_{OF}) defined as $E_{total}\,(ZrO_2)_n - n\,E_{total}\,(ZrO_2)$.

[d] Formation energy per unit of (ZrO_2) (E_{FPU}) defined as $[E_{total}\,(ZrO_2)_n - n\,E_{total}\,(ZrO_2)]/n$.

[e] Energy related to the most stable cluster.

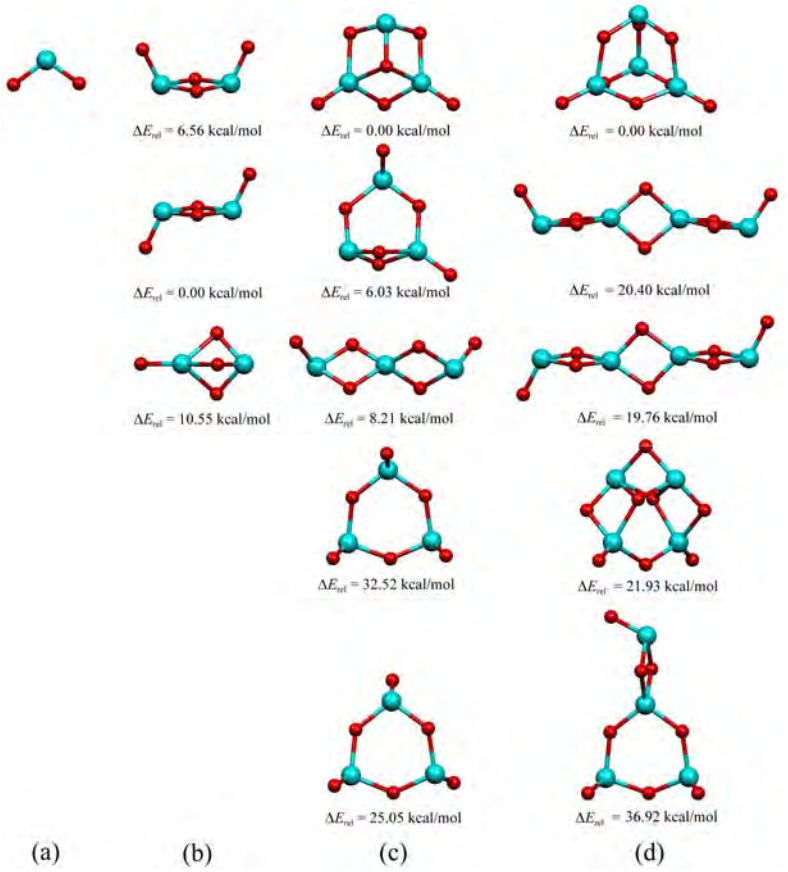

Figure A1 The B3LYP/GEN−optimized structures of, (a) (ZrO_2), (b) [$(ZrO_2)_2$_a, $(ZrO_2)_2$_b and $(ZrO_2)_2$_c], (c) [$(ZrO_2)_3$_a, $(ZrO_2)_3$_b, $(ZrO_2)_3$_c, $(ZrO_2)_3$_d, and $(ZrO_2)_3$_e], (d) [$(ZrO_2)_4$_a, $(ZrO_2)_4$_b, $(ZrO_2)_4$_c, $(ZrO_2)_4$_d, and $(ZrO_2)_4$_e], (e) [$(ZrO_2)_5$_a, $(ZrO_2)_5$_b, $(ZrO_2)_5$_c, $(ZrO_2)_5$_d, $(ZrO_2)_5$_e, $(ZrO_2)_5$_f, and $(ZrO_2)_5$_g], (f) [$(ZrO_2)_6$_a, $(ZrO_2)_6$_b, $(ZrO_2)_6$_c, $(ZrO_2)_6$_d, $(ZrO_2)_6$_e], $(ZrO_2)_6$_f, and $(ZrO_2)_6$_g], (g) [$(ZrO_2)_7$_a, $(ZrO_2)_7$_b and $(ZrO_2)_7$_c], (h) [$(ZrO_2)_8$_a, $(ZrO_2)_8$_b, $(ZrO_2)_8$_c, $(ZrO_2)_8$_d, and $(ZrO_2)_8$_e], (i) [$(ZrO_2)_9$_a, $(ZrO_2)_9$_b and $(ZrO_2)_9$_c], (j) [$(ZrO_2)_{10}$_a, $(ZrO_2)_{10}$_b, $(ZrO_2)_{10}$_c and $(ZrO_2)_{10}$_d], (k) [$(ZrO_2)_{11}$_a, $(ZrO_2)_{11}$_b and $(ZrO_2)_{11}$_c] and (l) [$(ZrO_2)_{12}$_a, $(ZrO_2)_{12}$_b, $(ZrO_2)_{12}$_c and $(ZrO_2)_{12}$_d]. Sequences for names of their conformers in square brackets correspond to the top to down clusters.

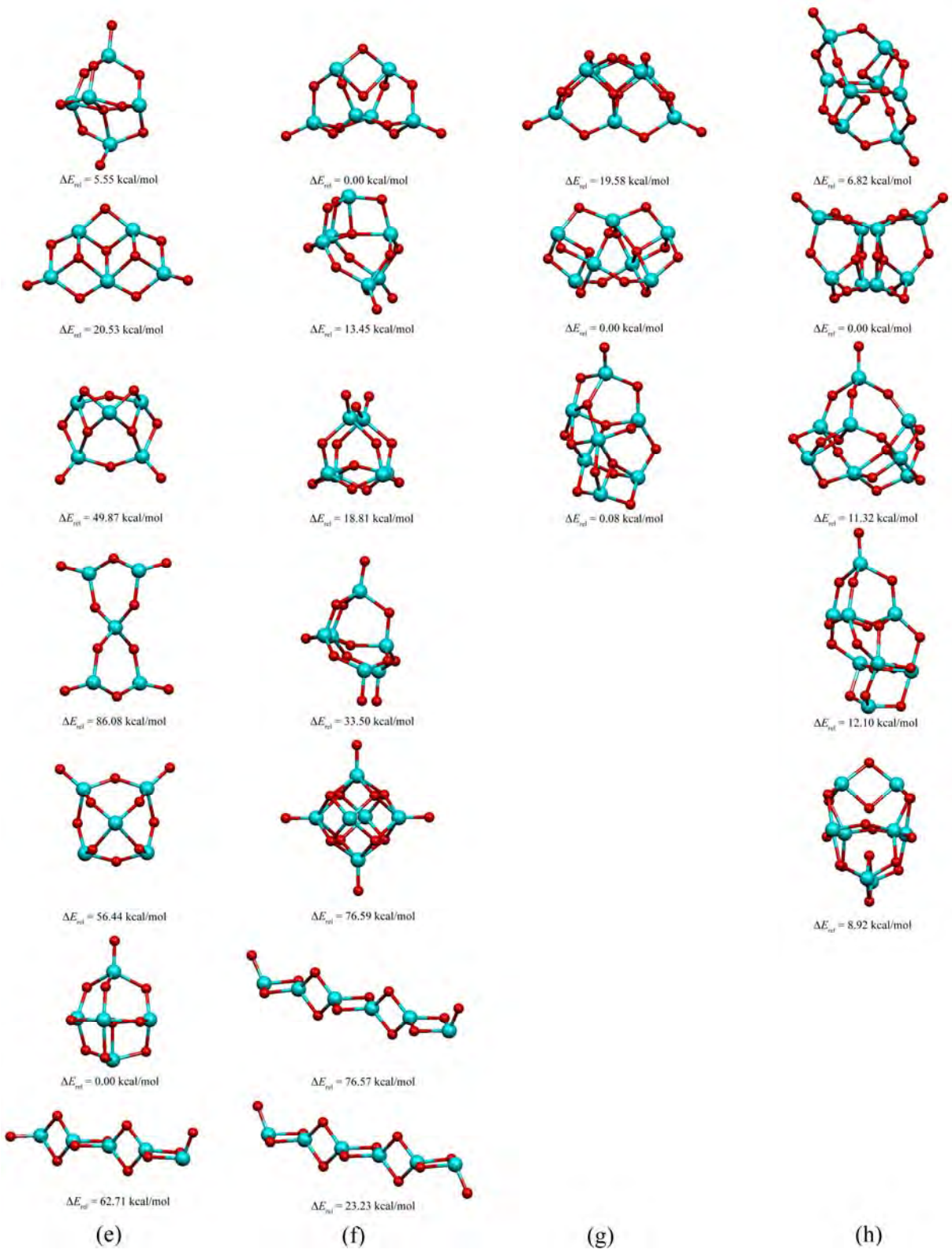

Figure A1 Continued.

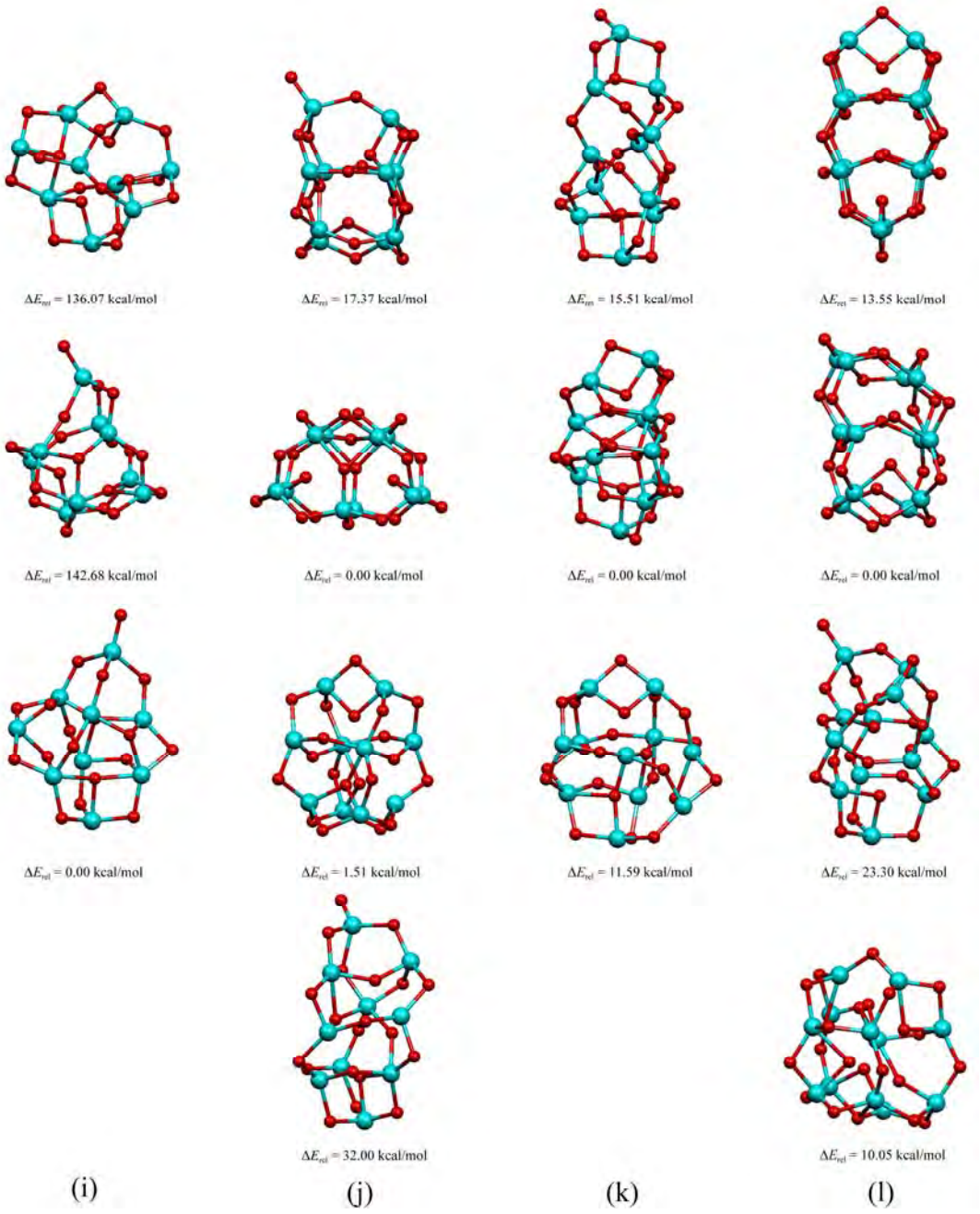

Figure A1 Continued.

Table A2 Configuration parameters for gas adsorption toward Zr adsorption–site atom on the ZrO_2–NP, computed at the B3LYP/GEN and M06–2X/GEN (in parenthesis) levels of theory.

Adsorption complexes	[X···Zr][a]		[Y–X···Zr][b]		[Y–X···Zr–O][c]	
	Site A	Site B	Site A	Site B	Site A	Site B
Diatomic						
H_2/ZrO_2–NP	2.77 (2.62)	3.06 (2.71)	83.2 (81.5)	84.8 (84.2)	0.01 (–5.2)	20.6 (–0.9)
N_2/ZrO_2–NP	2.66 (2.58)	2.79 (2.67)	179.0 (180.0)	176.5 (176.3)	–27.8 (–82.1)	16.3 (9.9)
O_2/ZrO_2–NP	2.50 (2.55)	2.53 (2.59)	118.0 (100.3)	119.1 (109.6)	–28.4 (–64.9)	2.0 (52.1)
O_2/ZrO_2–NP(t)[d]	2.69 (2.58)	2.95 (2.71)	126.5 (122.0)	121.1 (115.0)	63.9 (63.7)	–54.0 (–52.0)
O<u>C</u>/ZrO_2–NP	2.69 (2.65)	2.72 (2.69)	176.5 (179.0)	176.5 (175.5)	2.7 (52.6)	40.9 (26.8)
C<u>O</u>/ZrO_2–NP	2.61 (2.52)	2.86 (2.68)	179.2 (165.3)	165.8 (141.5)	21.4 (52.5)	37.1 (17.5)
O<u>N</u>/ZrO_2–NP	2.62 (2.61)	2.72 (2.68)	137.0 (126.6)	131.0 (124.9)	–50.8 (60.5)	–15.5 (12.1)
N<u>O</u>/ZrO_2–NP	2.67 (2.57)	3.18 (2.70)	129.6 (118.4)	120.7 (115.0)	21.4 (63.2)	60.0 (51.6)
Triatomic						
CO_2/ZrO_2–NP	2.51 (2.44)	3.16 (2.86)	136.4 (128.6)	108.3 (109.8)	–52.9 (48.4)	–13.1 (–14.5)
O<u>N_2</u>/ZrO_2–NP	2.55 (2.51)	2.73 (2.62)	176.0 (177.9)	164.2 (169.3)	–53.8 (52.8)	–56.2 (–29.4)
N_2<u>O</u>/ZrO_2–NP	2.52 (2.44)	2.68 (2.55)	78.3 (116.5)	117.4 (115.5)	–9.1 (–7.0)	19.5 (20.3)
O_2<u>N</u>/ZrO_2–NP	2.54 (2.47)	2.69 (2.58)	118.6 (114.3)	115.2 (109.8)	–20.2 (–22.8)	–48.5 (50.8)
H_2O/ZrO_2–NP	2.37 (2.33)	2.46 (2.43)	97.4 (118.1)	108.9 (98.0)	6.5 (–2.5)	–21.5 (–18.4)
H_2S/ZrO_2–NP	2.98 (2.90)	3.08 (2.98)	93.8 (90.3)	97.6 (92.6)	–7.0 (12.7)	–4.0 (55.3)
SO_2/ZrO_2–NP	2.28 (2.23)	2.59 (2.52)	106.1 (104.8)	118.0 (111.7)	2.9 (1.2)	38.8 (45.2)
Tetraatomic						
C_2H_2/ZrO_2–NP	2.90 (2.80)	3.20 (3.04)	101.2 (101.9)	65.7 (101.9)	0.1 (0.0)	–29.8 (–11.7)
C_2H_4/ZrO_2–NP	2.95 (2.83)	3.15 (3.06)	76.7 (102.5)	77.8 (105.8)	15.5 (–22.9)	0.8 (40.5)
CH_4/ZrO_2–NP	2.97 (2.77)	3.56 (3.16)	72.2 (73.1)	95.7 (88.7)	6.8 (0.8)	0.0 (–3.9)
H_3<u>N</u>/ZrO_2–NP	2.46 (2.42)	2.49 (2.46)	109.3 (111.6)	109.9 (107.0)	–0.5 (–7.2)	–9.5 (–2.7)

[a] Bond distance between the Zr of the ZrO_2–NP and the nearest gas atom (denoted by Z), in Å.
[b] Angle of two gas atoms (denoted by Y–X) and the Zr of the ZrO_2–NP, in degree.
[c] The smallest dihedral angle of between the nearest gas bond (denoted by Y–X) and of the Zr–O bond of the ZrO_2–NP, in degree.
[d] Triplet–state complex.

Table A3 The energy gaps of the ZrO2–NP and its gases adsorption complexes, computed at the B3LYP/GEN and M06–2X/GEN methods.

Configurations	$E_{gap,}$ at B3LYP/GEN		$E_{gap,}$ at M06–2X/GEN	
	At site A	At site B	At site A	At site B
ZrO_2–NP	5.719	–	8.365	–
Diatomic				
H_2/ZrO_2–NP	5.665	5.717	8.359	8.354
N_2/ZrO_2–NP	5.160	5.698	8.179	8.337
O_2/ZrO_2–NP	1.844	2.149	4.832	6.000
O_2/ZrO_2–NP(t)[d]	5.704	5.711	8.343	8.349
O<u>C</u>/ZrO_2–NP	4.967	5.689	7.924	8.328
C<u>O</u>/ZrO_2–NP	5.443	5.701	8.329	8.340
O<u>N</u>/ZrO_2–NP	3.060	3.195	6.517	6.717
N<u>O</u>/ZrO_2–NP	3.081	3.071	6.658	6.640
Triatomic				
CO_2/ZrO_2–NP	5.665	5.717	8.317	8.345
O<u>N_2</u>/ZrO_2–NP	5.264	5.684	8.227	8.320
N_2<u>O</u>/ZrO_2–NP	5.674	5.691	8.317	8.313
O_2<u>N</u>/ZrO_2–NP	3.773	4.693	7.160	8.182
H_2O/ZrO_2–NP	5.647	5.571	8.285	8.182
H_2S/ZrO_2–NP	5.645	5.520	8.298	7.811
SO_2/ZrO_2–NP	4.524	3.634	7.633	7.011
Tetraatomic				
C_2H_2/ZrO_2–NP	5.661	5.669	8.296	8.207
C_2H_4/ZrO_2–NP	5.540	5.552	8.298	7.751
CH_4/ZrO_2–NP	5.696	5.714	8.330	8.345
H_3<u>N</u>/ZrO_2–NP	5.569	5.584	8.231	8.216

[a] In eV.

Table A4 Energies of frontier orbitals and energy gaps of ZrO_2–NP doped by single metal atom, computed at the M06–2X/GEN level of theory.

Metal–doped ZrO_2–NPs	E_{HOMO}[a]	E_{LUMO}[a]	E_g[a]	ΔE_g,[b]
Non–doped	–9.756	–1.391	8.365	–
Sc–doped	–9.534	–1.583	7.951	4.94
Ti–doped	–9.696	–1.691	8.005	4.29
V–doped	–9.151	–1.978	7.174	14.24
Cr–doped	–8.870	–2.402	6.468	22.67
Mn–doped	–9.714	–2.670	7.044	15.79
Fe–doped	–9.693	–2.666	7.027	15.99
Co–doped	–[c]	–[c]	–[c]	–[c]
Ni–doped	–9.758	–4.097	5.661	32.33
Cu–doped	–[c]	–[c]	–[c]	–[c]
Zn–doped	–9.388	–1.913	7.475	10.63

[a] In eV.

[b] Difference between energy gaps of metal– and non–doped ZrO_2–NPs, in %.

[c] Due to no structure optimization is carried out, no data is obtained,

Table A5 Adsorption energies of hydrogen gas on metal–doped ZrO_2–NPs compared with non–doped ZrO_2–NP, computed at the M06–2X/GEN and M06–2X/GEN//B3LYP/GEN levels of theory.

H_2 adsorbed on M–doped ZrO_2–NPs	ΔE_{ads} [a]	
	M06–2X/GEN	M06–2X//B3LYP [b]
H_2/non–doped	–3.96	–3.93
H_2/Sc–doped	– [c]	–6.67
H_2/Ti–doped	–4.55	–4.57
H_2/V–doped	–5.43	–5.47
H_2/Cr–doped	– [c]	–6.15
H_2/Mn–doped	– [c]	–6.12
H_2/Fe–doped	–6.69	–6.86
H_2/Co–doped	– [c]	–5.19
H_2/Ni–doped	– [c]	–6.43
H_2/Cu–doped	– [c]	–2.93
H_2/Zn–doped	–4.26	–3.88

[a] In kcal/mol.

[b] Computed based on the rigid B3LYP/GEN–optimized structures of metal–doped ZrO_2–NP, $\Delta E_{ads} = E_{H_2/ZrO_2NP}$ (M06–2X/GEN//B3LYP/GEN) –[E_{ZrO_2NP} (M06–2X/GEN//B3LYP/GEN)– E_{H_2} (M06–2X/GEN)].

[c] No complete data is obtained.